Regulation of apical constriction via microtubule- and Rab11-dependent apical transport during tissue invagination

Thao Phuong Le[1] and SeYeon Chung[1, *]

[1] Department of Biological Sciences, Louisiana State University, Baton Rouge, LA 70803, USA

[*]Author for correspondence: seyeonchung@lsu.edu

Running Head: MTs and Rab11 regulate apical constriction

Abbreviations: Crb, Crumbs; E-Cad, E-Cadherin; Dhc64C, Dynein heavy chain 64C; Fog, Folded gastrulation; GFP, green fluorescent protein; Klar, Klarsicht; MT, microtubule; Nuf, Nuclear fallout; Rok, Rho-associated kinase; SG, salivary gland; WT, wild type; YFP, yellow fluorescent protein.

Abstract

The formation of an epithelial tube is a fundamental process for organogenesis. During *Drosophila* embryonic salivary gland (SG) invagination, Folded gastrulation (Fog)-dependent Rho-associated kinase (Rok) promotes contractile apical myosin formation to drive apical constriction. Microtubules (MTs) are also crucial for this process and are required for forming and maintaining apicomedial myosin. However, the underlying mechanism that coordinates actomyosin and MT networks still remains elusive. Here, we show that MT-dependent intracellular trafficking regulates apical constriction during SG invagination. Key components involved in protein trafficking, such as Rab11 and Nuclear fallout (Nuf), are apically enriched near the SG invagination pit in a MT-dependent manner. Disruption of the MT networks or knockdown of *Rab11* impairs apicomedial myosin formation and apical constriction. We show that MTs and Rab11 are required for apical enrichment of the Fog ligand as well as the apical determinant protein Crumbs (Crb) and the key adherens junction protein E-Cadherin (E-Cad). Targeted knockdown of *crb* or *E-Cad* in the SG disrupts apical myosin networks and results in apical constriction defects. Our data suggests a role of MT- and Rab11-dependent intracellular trafficking in regulating actomyosin networks and cell junctions, to coordinate cell behaviors during tubular organ formation.

41 **Introduction**

42 Formation of three-dimensional tubes by invagination of flat epithelial sheets is a
43 fundamental process in forming organs such as the lungs and kidneys (Andrew and
44 Ewald, 2010). To enter the third dimension, cells must change their shapes and positions
45 relative to each other. A major cellular process during epithelial tube formation is apical
46 constriction, a universal cell shape change that is linked to tissue bending, folding and
47 invagination (Martin and Goldstein, 2014; Sawyer et al., 2010). During apical constriction,
48 the apical side of an epithelial cell constricts, causing a columnar or cuboidal cell to
49 become wedge-shaped (Martin and Goldstein, 2014; Sawyer et al., 2010). Manipulation
50 of apical constriction in a group of cells impacts both local and global tissue shape directly,
51 suggesting a critical role for apical constriction in forming proper tissue architecture
52 (Chung et al., 2017; Guglielmi et al., 2015; Izquierdo et al., 2018).

53 Apical constriction is driven by actin filament (F-actin) networks and the molecular motor
54 non-muscle myosin II (hereafter referred to as myosin). Over the past decade, important
55 functions of different actomyosin structures in epithelial tissue morphogenesis have been
56 discovered. Particularly, studies in *Drosophila* revealed a distinct population of pulsatile
57 apical medial actomyosin (hereafter referred to as apicomedial myosin) that generates a
58 pulling force that exerts on adherens junctions to drive apical constriction (Booth et al.,
59 2014; Chung et al., 2017; Martin et al., 2009; Rauzi et al., 2010). Further studies in early
60 *Drosophila* embryos discovered that apicomedial myosin is created in response to
61 signaling by the Folded gastrulation (Fog) ligand and its G protein-coupled receptors
62 (GPCRs) (Kerridge et al., 2016; Manning et al., 2013) and is regulated by apical Rho-
63 associated kinase (Rok) (Mason et al., 2013).

64 Apical junctions and apical determinants also have an important role in the formation of
65 functional actomyosin complexes during developmental processes. During *Drosophila*
66 dorsal closure, the apical polarity regulators Par-6, aPKC and Bazooka/Par3 (Baz/Par3)
67 (altogether known as the Par complex) regulate pulsed actomyosin contractions in
68 amnioserosa cells (David et al., 2010). In the *Drosophila* embryonic trachea, the apical

protein Crumbs (Crb) is required for proper organization of the actomyosin complex (Letizia et al., 2011).

Emerging evidence suggests that microtubules (MTs) play a critical role in tissue invagination (Booth et al., 2014; Ko et al., 2019). MTs serve as tracks in intracellular transport (Aguilar-Aragon et al., 2020; Khanal et al., 2016; Le Droguen et al., 2015), raising the possibility that MTs regulate apical constriction through the endo- and exocytosis of membrane receptors and adhesion molecules. Several lines of evidence also suggest the importance of the endocytic pathway in apical constriction in both in vitro and in vivo systems. In *Drosophila* S2 cells, RhoGEF2 travels to the cell cortex by interaction with the MT plus-end protein EB1 to stimulate cell contraction (Rogers et al., 2004). During *Xenopus* gastrulation, disrupting endocytosis with dominant-negative dynamin or Rab5 perturbs apical constriction and invagination of cell sheets (Lee and Harland, 2010). During *Drosophila* gastrulation, the apical surface of cells is reshaped via Rab35 and RabGEF Sbf, which direct the plasma membrane to Rab11-positive recycling endosomes through a dynamic interaction with Rab5 endosomes to reshape actomyosin networks (Miao et al., 2019). Moreover, in the developing neural tube in *Xenopus*, asymmetric enrichment of Rab11 at the medial apical junctions is critical for apical constriction, suggesting that membrane trafficking has a key role in apical constriction (Ossipova et al., 2014). However, exactly how vesicle trafficking, MTs, and actomyosin networks are linked during tissue invagination remains to be discovered.

To determine how these three cellular attributes contribute to tissue invagination, we use the *Drosophila* embryonic SG as a model. We and others showed that apical constriction is regulated in a highly coordinated and spatiotemporally controlled manner during SG tube formation (Booth et al., 2014; Chung et al., 2017; Myat and Andrew, 2000; Sanchez-Corrales et al., 2018). The *Drosophila* embryo forms two SG tubes via invagination of two epithelial placodes on the ventral surface (Chung et al., 2014; Myat and Andrew, 2002). Before invagination, a small group of cells in the dorsal/posterior region of each SG placode begin to constrict. As those cells internalize to form the invagination pit, more cells anterior to the pit undergo clustered apical constriction in a Fog signaling-dependent manner (Chung et al., 2017) (Figure 1A). In the absence of *fog*, SG cells fail to accumulate

99 Rok and myosin in the apicomedial region of the cells (Chung et al., 2017). MTs aid in the
100 formation and maintenance of the apicomedial myosin network during SG invagination
101 (Booth et al., 2014). The MT cytoskeleton near the invagination pit forms a network of
102 longitudinal MT bundles, with the minus ends of MTs facing the apical domain of the cells
103 and interacting with the apicomedial myosin (Booth et al., 2014). Disruption of MTs
104 causes loss of apicomedial myosin and disrupted apical constriction during SG
105 invagination (Booth et al., 2014). However, it is still unknown how intracellular trafficking
106 affects these two processes.

107 In this study, we demonstrate that key proteins involved in intracellular trafficking -
108 including Rab11, its binding partner Nuclear fallout (Nuf), and dynein heavy chain - are
109 enriched in the apical domain of SG cells during invagination. Moreover, disruption of
110 MTs results in mislocalization of Rab11 to the basolateral region of SG cells. Reducing
111 *Rab11* in the SG leads to a decrease and a dispersal of Rok and myosin in the apical
112 domain and causes uncoordinated apical constriction. Our data suggest that apical
113 localization of the Fog ligand, the apical determinant protein Crb, and the key adherens
114 junction protein E-Cadherin (E-Cad) is compromised when the MT networks are disrupted
115 or *Rab11* is knocked down. We further show that reducing *crb* or *E-Cad* in the SG leads
116 to defects that are reminiscent of *Rab11* knockdown. Altogether, our work mechanistically
117 links MT- and Rab11-dependent intracellular trafficking to the regulation of actomyosin
118 networks during tubular organ formation.

119

120 Results

121 Intracellular trafficking components are apically enriched near the invagination pit

122 To test a role for the intracellular trafficking machinery in spatially biased signaling
123 activation and protein accumulation during SG invagination, we analyzed the subcellular
124 localization of proteins that are involved in vesicle trafficking in the SG. Several endosome
125 markers and their interacting partners were tested, including Rab5 (an early endosome
126 marker) (Gorvel et al., 1991), Rab7 (a late endosome marker) (Meresse et al., 1995;

127 Wichmann et al., 1992), Rab11 (a recycling endosome marker) (Ullrich et al., 1996),
128 Nuclear fallout (Nuf, a putative binding partner for Rab11) (Riggs et al., 2003), and Sec15
129 (an exocyst complex component and effector for Rab11) (Langevin et al., 2005; Zhang et
130 al., 2004). Using labeling with E-Cad, an adherens junction marker, and CrebA, a SG
131 nuclear marker, we segmented apical cell outlines and calculated intensity mean of
132 fluorescence signals of each endosomal marker. We observed apical enrichment of
133 several of them in the SG, including Rab11 and Nuf (Figure 1, B-B''''). Similar enrichment
134 of Rab11 signals was also observed in the endogenously tagged Rab11 protein (Rab11-
135 EYFP; (Dunst et al., 2015) (Supplemental Figure S1, A-A''''). Importantly, the enrichment
136 of Rab11 was more pronounced in the SG over time (Figure 1, D-F''''). Before
137 invagination, only low levels of Rab11 were detected in the apical domain of all SG cells
138 throughout the entire SG placode (Figure 1, D-D''''). Stronger signals of Rab11 were soon
139 detected in the SG as cells begin to undergo apical constriction in the dorsal/posterior
140 region of the placode (Figure 1, E-E''''), which intensified as invagination proceeded
141 (Figure 1, F-F''''). Quantification of the total intensity of Rab11 in the whole SG placode
142 showed significantly higher levels of Rab11 in invaginating SGs compared to before
143 invagination (Figure 1H), suggesting upregulated Rab11 levels in SG cells during
144 invagination. Furthermore, compared to before invagination (Figure 1G, top), intensity
145 mean of Rab11 in the apical domain of each cell showed a stronger negative correlation
146 with the apical area of cells in the entire SG during invagination (Figure 1G, bottom),
147 suggesting a close link between intracellular trafficking activities and apical constriction.

148 EYFP-tagged Rab5, an early endosome marker, was also enriched in the apical domain
149 in the invaginating SG, suggesting active endocytosis in the apical domain during SG
150 invagination (Supplemental Figure S1, B-B'''). Rab7, a late endosome marker, however,
151 did not show apical enrichment but localized as large punctate structures in the cytoplasm
152 of the entire SG placode (Supplemental Figure 1, D-D'''). Dynein heavy chain 64C, a
153 subunit of the dynein motor complex that transports cargos along MTs toward their minus
154 ends, also showed apical enrichment (Figure 1, C-C'''). This is consistent with previous
155 report that the minus end of MTs faces the apical domain of SG cells near the invagination
156 pit (Booth et al., 2014). Sec15, an exocyst complex component, also showed similar
157 apical enrichment (Supplemental Figure S1, E-E'''). Similar to Rab11 (Figure 1G),

158 intensity mean of Rab5-EYFP and Sec15 in the apical domain of each cell showed a
159 negative correlation with the apical area of cells in the entire SG during invagination
160 (Supplemental Figure S1, C and F). Compared to a more uniform distribution of other
161 endosomal markers in the entire apical domain of SG cells, Sec15 signals appeared to
162 be enriched at adherens junctions (Supplemental Figure S1E'). Overall, our results
163 suggest active intracellular trafficking, possibly both endo- and exocytosis, in the apical
164 domain of SG cells near the invagination pit during invagination.

165

166 **Apical enrichment of Rab11 and Nuf is MT-dependent**

167 Strong apical enrichment of Rab11 and other trafficking components in SG cells near the
168 invagination pit led us to test whether these vesicle markers are associated with vertically
169 aligned MTs that could facilitate their polarized distribution. As in many epithelial cells,
170 MT minus- and plus-ends face the apical and the basal domain of the SG cells,
171 respectively (Booth et al., 2014; Myat and Andrew, 2002). Indeed, co-immunostaining of
172 tyrosinated α-tubulin, a marker of dynamic or newly polymerized MTs (Westermann and
173 Weber, 2003), and Rab11 showed a partial overlap of the two proteins at the apical region
174 of the SG cells (Figure 2, A-B'').

175 To test whether Rab11 apical enrichment in SG cells is dependent on MT networks, we
176 disrupted MTs in the SG by overexpressing spastin, a MT-severing protein (Sherwood et
177 al., 2004), using the SG-specific *fkh-Gal4* driver. In control SGs, tyrosinated α-tubulin and
178 acetylated α-tubulin, a marker of stable and longer-lived MTs (Westermann and Weber,
179 2003), were observed abundantly in the apical domain of cells in the whole placode
180 (Figure 2, C'' and C'''; Supplemental Figure S2A''). In spastin-overexpressing SGs, both
181 tyrosinated and acetylated α-tubulin signals were strongly reduced, revealing loss of MT
182 filaments (Booth et al., 2014) (Figure 2, D'' and D''' and Supplemental Figure S2B''). The
183 apical enrichment of Rab11 (Figure 2C') was also disrupted and Rab11 was mislocalized
184 basolaterally (Figure 2D'). SGs with disrupted MTs showed much lower Rab11 and Nuf
185 intensity in the apical domain compared to control SGs (Figure 2, E-G). To compare the
186 relative variability of apical enrichment of Rab11/Nuf in WT and spastin-overexpressing

SGs, we calculated coefficient of variation, the ratio of standard deviation of Rab11/Nuf intensity to the mean Rab11/Nuf intensity. Compared to WT, spastin-overexpressing SGs showed a lower degree of relative variability of intensity (Figure 2G). Overall, these data suggest that MT networks are required for apical enrichment of Rab11 and Nuf during SG invagination.

Rab11 and dynein functions are required for apical constriction in the SG

We next asked if modulation of Rab11 levels could compromise apical constriction. To test this possibility, we disrupted the function of Rab11 in the SG by either overexpressing a dominant-negative form of Rab11 (Rab11S25N-YFP; (Zhang et al., 2007); hereafter referred to as Rab11-DN) or knocking down *Rab11* using RNAi lines. Reduced Rab11 levels upon *Rab11* knockdown were confirmed using a Rab11 antibody in both stage 11 and stage 13 SGs (Supplemental Figure S3, A-D'). Compared to control (Figure 3A), SGs overexpressing Rab11-DN or knocking down *Rab11* showed more cells with larger apical areas (Figure 3, B, C and F), suggesting a role for Rab11 in apical constriction during SG invagination.

As dynein heavy chain was also enriched apically in the SG during invagination (Figure 1, C' and C'''), we tested if dynein function is also required for apical constriction during SG invagination. Indeed, knockdown of *Dynein heavy chain 64C* (*Dhc64C*) in the SG using RNAi resulted in more cells with larger apical areas during invagination, suggesting defective apical constriction upon *Dhc64C* knockdown (Figure 3, D, D' and G). As dynein binds to and clusters the minus ends of microtubules (Burbank et al., 2006; Elting et al., 2014; Goshima et al., 2005; Heald et al., 1996; Khodjakov et al., 2003; Tan et al., 2018), we asked if *Dhc64C* knockdown affects the MT networks in the SG. Knocking down *Dhc64C* in the SG resulted in a slight reduction of tyrosinated α-tubulin (Figure 3J'). These data suggest that apical constriction defects observed in *Dhc64C* knockdown is, at least in part, due to affected MT networks.

214 Klarsicht (Klar), the *Drosophila* Klarsicht-Anc-Syne Homology (KASH) domain protein,
215 mediates apical transport in the SG (Myat and Andrew, 2002) via the MT motor
216 cytoplasmic dynein (Gross et al., 2000). We therefore tested if *klar* also influences apical
217 constriction during SG invagination. *klar* null mutant embryos showed SGs with mild
218 apical constriction defects compared to wild type (Figure 3, E-F' and H). Importantly,
219 unlike *Dhc64C* knockdown, no significant difference in the MT networks was observed in
220 SGs in *klar* mutants (Figure 3L'), suggesting that apical constriction defects in *klar*
221 mutants are due to disrupted apical transport. Overall, our data suggest essential roles of
222 MT-, Rab11- and dynein-dependent intracellular transport in regulating apical constriction
223 during SG invagination.

224

225 **Reduced Rab11 function leads to reduction of apicomedial myosin formation and**
226 **failure in accumulation of apicomedial Rok in SG cells**

227 The apicomedial myosin structure generates the pulling force to drive apical constriction
228 in SG cells (Booth et al., 2014; Chung et al., 2017). Disruption of MTs by spastin
229 overexpression inhibits formation of apicomedial myosin during SG invagination (Booth
230 et al., 2014). To test whether apicomedial myosin is affected in SG cells when *Rab11* is
231 knocked down, we measured the overall intensity of myosin in the apicomedial region of
232 SG cells using sqh-GFP, a functional GFP-tagged version of the myosin regulatory light
233 chain (Royou et al., 2004). In control SGs, sqh-GFP showed strong myosin signals with
234 clear web-like structures in the apicomedial region of cells near the invagination pit
235 (Figure 4, A-A''''). Knockdown of *Rab11*, however, caused a significant reduction of
236 apicomedial myosin intensity in SG cells in the same area (Figure 4, B-B'''' and C).
237 Moreover, unlike clear web-like structures of apicomedial myosin in control SGs (Figure
238 4, A''-A''''), myosin was more dispersed and fragmented in *Rab11* RNAi SGs (Figure 4,
239 B''-B''''), resulting in a decrease in areas of myosin accumulation in the apicomedial
240 region of SG cells (Figure 4E). These data suggest roles for Rab11 in both upregulating
241 apical myosin and forming and/or maintaining apicomedial myosin web.

242 We also tested whether junctional myosin, a myosin pool that is closely associated with
243 adherens junctions in SG cells, is affected in *Rab11* RNAi SGs. Consistent with previous
244 studies (Chung et al., 2017; Roper, 2012), junctional myosin showed strong signals in
245 wild type SG cells, often with stronger signals at vertices (Figure 4A'''). Intriguingly, the
246 intensity of junctional myosin slightly increased when *Rab11* was knocked down (Figure
247 4, B''' and D). The ratio of apicomedial to junctional myosin intensity was significantly
248 reduced in *Rab11* RNAi SGs (Figure 4D), suggesting imbalance of contractile forces in
249 the SG.

250 We previously showed that accumulation of apicomedial Rok is required for apicomedial
251 myosin formation for coordinated apical constriction in SG cells (Chung et al., 2017;
252 Roper, 2012). To test whether Rok accumulation is dependent on Rab11, we quantified
253 accumulation of apicomedial Rok-GFP signals using a ubiquitously expressed GFP-
254 tagged Rok transgene (Rok-GFP; (Abreu-Blanco et al., 2014) in wild type and *Rab11*
255 RNAi SGs (Figure 4, F-G''). Indeed, reduction of *Rab11* levels led to more dispersed Rok
256 signals along the apical domain of SG cells near the pit (Figure 4H). Overall, our data
257 suggest Rab11-dependent apical apicomedial myosin formation and accumulation of Rok
258 during SG invagination.

259

260 **Reduced dynein function leads to failure in proper organization of apicomedial**
261 **myosin in SG cells**

262 We next tested whether apicomedial myosin formation is affected in *Dhc64C* RNAi and
263 *klar* mutant SGs. Despite slight disruption of the MT networks in *Dhc64C* RNAi SGs
264 (Figure 3J'), the overall intensity of apicomedial or junctional myosin was not significantly
265 changed in *Dhc64C* RNAi SGs (Figure 5C), suggesting that subtle defects in the MT
266 networks do not affect apical upregulation of myosin. Similar to *Dhc64C* knockdown, no
267 significant difference in the intensity of apicomedial and junctional myosin was observed
268 in *klar* mutant SGs (Figure 5H). However, the ratio of apicomedial to junctional myosin
269 was reduced in both genotypes (Figure 5, D and I). Moreover, the area of apicomedial
270 myosin accumulation was significantly reduced in *Dhc64C* RNAi or *klar* mutant SGs

271 (Figure 5, E and J), suggesting defects in forming proper apicomedial myosin web in
272 these genotypes. Our data suggests that defective apical constriction in *Dhc64C* RNAi
273 and *klar* mutant SGs could be due to failure in proper organization of myosin structures
274 in SG cells.

275 We also tested for accumulation of apicomedial Rok-GFP signals in spastin-
276 overexpressing, *Dhc64C* RNAi and *klar* mutant SGs. Disruption of MTs by spastin
277 overexpression abolished apicomedial accumulation of Rok in cells near the invagination
278 pit (Figure 5, L' and P), found in control SGs (Figure 5K'). Reduction of *Dhc64C* levels
279 also led to more dispersed Rok signals along the apical domain of SG cells near the pit
280 (Figure 5, M' and P). In *klar* mutants, Rok-GFP tended to accumulate less profoundly and
281 less uniformly in the apicomedial region of SG cells (Figure 5O') although not statistically
282 significant compared to control (Figure 5Q). Overall, our data suggest that MT- and
283 dynein-dependent apical accumulation of Rok and apicomedial myosin formation during
284 SG invagination.

285

286 **MT- and Rab11-dependent apical enrichment of Fog, Crb and E-Cad is required for**
287 **apical constriction during SG invagination**

288 We next tested potential cargos of MT- and Rab11-dependent apical transport during SG
289 invagination. Rok accumulation, apicomedial myosin formation and subsequent clustered
290 apical constriction in the SG is dependent on Fog signaling (Chung et al, 2017). We
291 therefore tested if apical transport of the Fog ligand is MT- and Rab11-dependent.
292 Staining using an antibody against Fog in control SGs showed upregulated Fog signals
293 in the apical domain of SG cells (Figure 6, A-A'''). However, in spastin-overexpressing or
294 *Rab11* RNAi SGs, apical Fog signals were reduced (Figure 6, B-C'''). To compare apical
295 enrichment of Fog between WT and spastin-overexpressing or *Rab11* RNAi SGs, we
296 calculated the overall intensity of apical Fog signals in the entire SG placode in
297 corresponding genotypes. Compared to control, Fog levels in the apical domain of the
298 SG were reduced when spastin was overexpressed or *Rab11* was knocked down (Figure
299 6G). We also calculated coefficient of variation, the ratio of standard deviation of Fog

300 intensity to the mean intensity of Fog in the SG. Compared to WT, spastin-overexpressing
301 or *Rab11* RNAi SGs had a lower degree of relative variability of intensity (Figure 6H).
302 These data suggest that apical transport of Fog in the SG is dependent of the MT
303 networks and Rab11.

304 We further tested MT- and Rab11-dependent apical transport of other apical and
305 junctional proteins during SG invagination. Transport of several key apical and junctional
306 proteins is dependent on MTs and Rab11 (Jouette et al., 2019; Khanal et al., 2016; Le
307 Droguen et al., 2015). One such protein is an apical transmembrane protein Crb, and
308 Rab11 helps maintain apical Crb in the *Drosophila* ectoderm (Roeth et al., 2009). In the
309 *Drosophila* SG and follicle cells, Crb is apically transported along MTs by the dynein motor
310 (Myat and Andrew, 2002). Importantly, in *Drosophila* tracheae, loss of *crb* impairs apical
311 constriction during the internalization process (Letizia et al., 2011). The key junctional
312 protein E-Cad is also trafficked by MTs in *Drosophila* embryonic trachea (Le Droguen et
313 al., 2015). During apical constriction, contractile forces generated by the actomyosin
314 complex are exerted on adherens junctions, with E-Cad being a core component that
315 integrates contractile forces to generate tension (Martin et al., 2009).

316 We therefore asked if MTs and Rab11 have roles in apical enrichment of Crb and E-Cad
317 in the SG during invagination. Compared to control (Figure 6, D' and D'''), spastin-
318 overexpressing SG cells showed discontinuous Crb signals (Figure 6, E' and E''').
319 Although the number of gaps was not significantly different between control and spastin-
320 overexpressing SGs (Figure 6H), the ratio of the length of gap over junctional length was
321 significantly increased in SGs that overexpress spastin (Figure 6H). Moreover, whereas
322 E-Cad signals were mainly detected at adherens junctions (Figure 6D''), disruption of MTs
323 resulted in mislocalization of E-Cad to the basolateral region (Figure 6E''). Importantly,
324 *Rab11* knockdown resulted in similar E-Cad mislocalization and discontinuous Crb
325 signals (Figure 6, F-F'''' and H). These data suggest that apical enrichment of Crb and E-
326 Cad in the invaginating SG is dependent on MTs and Rab11.

327 To test for a role of Crb and E-Cad in regulating apical constriction during SG invagination,
328 we knocked down either gene in the SG using RNAi. Knockdown of *crb* or *E-Cad* resulted

329 in reduction of junctional Crb or E-Cad levels, respectively, compared to control
330 (Supplemental Figure S3, E-F''). Reduction of *crb* or *E-Cad* increased the number of cells
331 that have larger apical areas compared to control (Figure 7, A-D'). Quantification of the
332 percentage of cells and cumulative percentage of cells of different apical areas showed
333 a significant decrease in the number of constricting cells in *crb* knockdown SGs (Figure
334 7D). *E-Cad* knockdown SGs also displayed a similar trend although with less statistical
335 significance (Figure 7D). These data suggest roles for Crb and E-Cad in regulating apical
336 constriction during SG invagination.

337

338 **Apical localization of Fog, Crb and E-Cad is MT- and Rab11-dependent in the SG**
339 **throughout development**

340 To further investigate the role of MTs in Rab11-dependent apical trafficking during SG
341 development, we overexpressed spastin in the SG throughout development and analyzed
342 late stage SGs. Analysis of spastin-overexpressing SGs at stage 16 revealed that
343 disruption of MTs resulted in short SG tubes with a thin lumen compared to control SGs
344 of the same stage (Supplemental Figure S5, A and B). Strikingly, whereas the majority of
345 Rab11- and Nuf-positive vesicles localized in the apical region of control SG cells
346 (Supplemental Figure S5, A-A'''), Rab11 and Nuf were observed as large aggregates in
347 the cytoplasm in spastin-overexpressing cells, overlapping with each other (Supplemental
348 Figure S5, B-B'''). Our data suggest that MTs are required for apical enrichment of
349 Rab11/Nuf vesicles throughout SG tube formation.

350 We next tested whether MTs and Rab11 are required for apical transport of Fog, Crb and
351 E-Cad also at later stages. Compared to the control SG (Supplemental Figure S5C''),
352 apical Fog signals were significantly reduced in SGs that overexpress spastin or knock
353 down *Rab11* (Supplemental Figure S5, D'' and E''), suggesting that Fog is trafficked
354 apically in a MT- and Rab11-dependent manner in the SG throughout tube formation. No
355 significant changes were detected in apical Crb localization in SGs that overexpress
356 spastin or knock down *Rab11* (data not shown). Compared to strong E-Cad enrichment
357 in adherens junctions in control SG cells (Supplemental Figure S5C'), SGs that

358 overexpress spastin or knock down *Rab11* showed stronger E-Cad signals in the lateral
359 domain of cells (Supplemental Figure S5, D' and E').

360 To further test MT-dependent apical transport of Crb or E-Cad in the SG, we used a
361 genetic suppression strategy in the overexpression background: we co-overexpressed
362 Crb or E-Cad along with spastin in the SG to test whether disruption of MTs affects apical
363 transport of Crb or E-Cad. A similar approach was taken in a recent study, where
364 overexpression of Crb provided a highly sensitive genetic background for identifying
365 components involved in Crb trafficking (Aguilar-Aragon et al., 2020). Consistent with
366 previous studies (Chung and Andrew, 2014; Wodarz et al., 1993), Crb overexpression in
367 the SG caused a dramatic increase of the apical membrane as well as mislocalization of
368 Crb basolaterally along the entire membrane (Supplemental Figure S4, F-F'). Co-
369 overexpression of spastin along with Crb suppressed the overexpression phenotypes for
370 Crb (Supplemental Figure S4, G-G'). E-Cad overexpression in the SG caused
371 mislocalization of E-Cad as punctate structures in the basolateral region (Supplemental
372 Figure S4, H'-H''). Importantly, in SGs that co-overexpressed spastin along with Crb or
373 E-Cad, each protein mislocalized as cytoplasmic aggregates near the basolateral domain,
374 which were largely overlapping with mislocalized Rab11/Nuf (Supplemental Figure S4,
375 G'-G''' and I'-I'''). Overall, our data suggest that Fog, Crb and E-Cad are trafficked apically
376 in a MT- and Rab11-dependent manner in the SG throughout tube formation.

377

378 **Reducing apical and junctional proteins affects apicomedial myosin formation**

379 To test whether apical constriction defects observed in *crb* and *E-Cad* RNAi SGs are
380 linked to apicomedial myosin formation, we quantified myosin levels and areas of
381 apicomedial myosin in SGs with these knockdowns. Compared to control SGs (Figure 8,
382 A-A''), *crb* RNAi SGs showed a slight decrease in apicomedial myosin levels (Figure 8,
383 B-B'' and D). No significant difference in the junctional myosin intensity was observed in
384 *crb* RNAi SGs (Figure 8, B-B'' and D). The ratio of apicomedial to junctional myosin was
385 reduced (Figure 8E), suggesting that apical constriction defects in SGs depleted of *crb*
386 are, at least in part, due to failure of apicomedial myosin formation. Supporting this idea,

387 areas of apicomedial myosin web-like structures were significantly reduced in *crb* RNAi
388 SGs compared to WT (Figure 8F).

389 In SGs knocked down *E-Cad*, myosin levels at each domain did not change significantly
390 (Figure 8, C-C'' and E), but areas of apicomedial myosin web-like structures were
391 significantly decreased (Figure 8F). The ratio of apicomedial to junctional myosin was
392 also significantly reduced in *E-Cad* RNAi SGs compared to control (Figure 8, C-C'' and
393 E). Therefore, apical constriction defects caused by *E-Cad* knockdown might be due to
394 defective apicomedial myosin formation and the imbalance of contractile forces.

395 Consistent with reduced apicomedial myosin (Figure 8, B' and D), knockdown of *crb* also
396 resulted in Rok-GFP signals less accumulating in the apical region of cells near the
397 invagination pit (Figure 8, F-G'). Quantification of areas occupied by Rok-GFP puncta
398 showed significant reduction in accumulation of apicomedial Rok when *crb* was knocked
399 down (Figure 8I). Consistent with little effect of *E-Cad* knockdown on apicomedial myosin
400 intensity (Figure 8, C-C'' and E), Rok accumulation was not significantly affected by *E-*
401 *Cad* knockdown (Figure 8, H-H' and I). Taken together, our results suggest a role for Crb
402 and E-Cad in regulating apical constriction by apicomedial myosin activation during SG
403 invagination.

404

405 **Discussion**

406 **MTs and Rab11 regulate Fog signaling activity during SG invagination**

407 MTs have a crucial role in stabilizing apical myosin during epithelial morphogenesis both
408 in early *Drosophila* embryos and in the *Drosophila* SG (Booth et al., 2014; Ko et al., 2019).
409 In the SG, MTs interact with apicomedial myosin via Short stop, the *Drosophila*
410 spectraplakin, emphasizing a direct interplay between the MT and the apical myosin
411 networks (Booth et al., 2014). Our data reveals another key role of MTs in regulating
412 protein trafficking to control the apical myosin networks during tissue invagination. During
413 SG invagination, a network of longitudinal MT bundles is observed near the invagination
414 pit (Booth et al., 2014). Our data shows apical enrichment of Rab11 in the same area is

415 MT-dependent (Figures 1 and 2) and that this enrichment is important for forming the
416 apicomedial myosin networks (Figure 4), suggesting a link between localized intracellular
417 trafficking along MTs to apical myosin regulation.

418 The dorsal/posterior region of the SG, where Rab11 is apically enriched in a MT-
419 dependent manner (Figures 1 and 2), correlates with localized Fog signaling activity that
420 promotes clustered apical constriction (Chung et al., 2017). Disruption of MTs or *Rab11*
421 knockdown reduces Fog signals in the apical domain of SG cells (Figure 6) and causes
422 dispersed Rok accumulation and defective apicomedial myosin formation (Figure 4). It is
423 consistent with our previous study that absence of Fog signal results in dispersed apical
424 Rok and defects in apicomedial myosin formation (Chung et al., 2017). We therefore
425 propose that MT- and Rab11-dependent apical trafficking regulates Fog signaling activity
426 to control apical constriction during epithelial tube formation, through transporting the Fog
427 ligand. As recycling of membrane receptors to the cell surface plays an important role in
428 the regulation of overall signaling activity, it is possible that Rab11 is involved in recycling
429 of the as yet unidentified SG receptor(s) of Fog to regulate Fog activity in the SG. Indeed,
430 several GPCRs are recycled via Rab11 (Anborgh et al., 2000; Cerniello et al., 2017; Dale
431 et al., 2004; Fan et al., 2003; Hamelin et al., 2005; Hunyady et al., 2002; Innamorati et
432 al., 2001; Volpicelli et al., 2002). During epithelial invagination in early *Drosophila*
433 embryogenesis, the concentration of the Fog ligand and receptor endocytosis by β-
434 arrestin-2 have been shown as coupled processes to set the amplitude of apical Rho1
435 and myosin activation (Jha et al., 2018). It is possible that the movement of Fog
436 receptor(s) that have internalized as a stable complex with β-arrestin is recycled back to
437 the cell surface by Rab11. The Fog signaling pathway represents one of the best-
438 understood signaling cascades controlling epithelial morphogenesis (Manning and
439 Rogers, 2014). Although best studied in *Drosophila*, the pathway components have been
440 also identified in other insects, suggesting a more widely conserved role of Fog signaling
441 in development (Benton et al., 2019; Urbansky et al., 2016). Further work needs to be
442 done to fully understand the regulatory mechanisms underlying trafficking of Fog and its
443 receptor(s) during epithelial morphogenesis.

444 Our analysis of apicomedial myosin shows that reduced Rab11 function not only causes
445 a decrease of the myosin intensity but also causes myosin to be dispersed rather than
446 forming proper myosin web structures in the apicomedial domain of SG cells (Figure 4).
447 These data support the idea that Rab11 function is required for both concentration and
448 spatial organization of apicomedial myosin. This can be explained by the combined effect
449 of multiple cargos that are transported by Rab11, including Fog, Crb and E-Cad (as
450 discussed below). Time-lapse imaging of myosin will help determine how dynamic
451 behavior of apicomedial myosin is compromised when Rab11 function is disrupted.

452

453 **Integrating apical and junctional proteins with actomyosin networks during SG**
454 **invagination**

455 During branching morphogenesis in *Drosophila* trachea, MTs and dynein motors have a
456 critical role in proper localization of junctional proteins such as E-Cad (Le Droguen et al.,
457 2015). This is consistent with our observations with MT-dependent apical localization of
458 E-Cad in the invaginating SG (Figure 6), suggesting a conserved role of MT-dependent
459 intracellular trafficking in junctional remodeling and stabilization during epithelial tube
460 formation. Our data further suggests that the MT networks and Rab11 have key roles in
461 apical localization of Crb and E-Cad in the SG (Figure 6) and that proper levels of apical
462 and junctional proteins are important for apical constriction during SG invagination (Figure
463 7). Based on these data, we propose that MT- and Rab11-dependent apical trafficking of
464 Crb and E-Cad is critical for apical constriction during SG invagination. Alternatively, MTs
465 have additional role in assembling/anchoring these apical components, through
466 regulation of unidentified molecules. Recent studies in *Drosophila* mesoderm invagination
467 showed that MTs help to establish actomyosin network linked to cell junction to facilitate
468 efficient force transmission to promote apical constriction (Ko et al., 2019). In Ko et al.,
469 (2019), however, MT-interfering drugs and RNAi of CAMSAP end-binding protein were
470 used to prevent MT functions and the effect cannot be directly compared to our data
471 where spastin was used to sever existing MTs. Direct monitoring MT-dependent transport
472 of Crb and E-Cad during SG invagination will help clarify the mechanism.

473 Upon knockdown of *crb* or *E-Cad,* less prominent apicomedial myosin web structures are
474 observed in invaginating SGs (Figure 8), suggesting a requirement of Crb and E-Cad in
475 proper organization of apical actomyosin networks during SG tube formation. Crb acts as
476 a negative regulator of actomyosin dynamics during *Drosophila* dorsal closure (Flores-
477 Benitez and Knust, 2015) and during SG invagination (Roper, 2012). It is possible that
478 proper Crb levels are required for modulating myosin activity both in the apicomedial
479 domain and at junctions during SG invagination, which contribute to apical constriction
480 and cell rearrangement, respectively (Roper, 2012; Sanchez-Corrales et al., 2018).
481 Anisotropic localization of Crb and myosin was observed at the boundary of the SG
482 placode, where myosin accumulates at edges where Crb is lowest (Roper, 2012). Planar
483 polarization of Rok at this boundary is modulated through phosphorylation by Pak1
484 downstream of Crb (Sidor et al., 2020). Further test will help understanding whether and
485 how Crb might affect junctional myosin dynamics and SG invagination. As contractile
486 actomyosin structures exert forces on adherens junction to drive apical constriction, we
487 speculate that apical constriction defects upon *E-Cad* RNAi might be due to reduction of
488 cell adhesion and/or of improper force transmission. It will be interesting to determine if
489 coordination of apical and junctional proteins and apical cytoskeletal networks through
490 intracellular trafficking is conserved during tubular organ formation in general.

491

492 **A role for dynein in apical constriction**

493 Dhc is also apically enriched in the dorsal/posterior region of the invaginating SG (Figure
494 1). Our data shows that knockdown of *Dhc64C* not only affect Rok accumulation and
495 apicomedial myosin formation (Figure 5) but also disrupts MT organization in the SG
496 (Figure 3). This data is consistent with previous findings that cytoplasmic dynein is
497 associated with cellular structures and exerts tension on MTs. For example, dynein
498 tethered at the cell cortex can apply a pulling force on the MT network by walking towards
499 the minus end of a MT (Laan et al., 2012). Dynein also scaffolds the apical cell cortex to
500 MTs to generate the forces that shape the tissue into a dome-like structure (Takeda et

501 al., 2018). In interphase cells, force generated by dynein also regulates MT turnover and
502 organization (Yvon et al., 2001).

503 In *klar* mutants, on the other hand, MT organization is not affected in the SG (Figure 3),
504 suggesting that reduction of dynein-dependent trafficking by loss of *klar* does not cause
505 changes in the MT networks. Notably, although the intensity of apicomedial myosin does
506 not change upon *Dhc64C* knockdown or in the *klar* mutant background, formation of
507 apicomedial myosin web structures is affected (Figure 5). These data suggest a possible
508 scenario that dynein function is not required for concentration of myosin in the apical
509 domain but is only needed for spatial organization of apicomedial myosin. We cannot rule
510 out the possibility, however, that zygotic knockdown of *Dhc64C* by RNAi is not strong
511 enough to affect the intensity of apicomedial myosin. *Dhc64C* has strong maternal
512 expression and is essential for oogenesis and early embryo development (Li et al., 1994).
513 Embryos with reduced maternal and zygotic pools of *Dhc64C* showed a range of
514 morphological defects in the entire embryo, some of which were severely distorted (data
515 not shown). Precise roles for dynein and dynein-dependent trafficking in regulating
516 apicomedial myosin formation remain to be elucidated.
517

518 **Materials and Methods**

519 **Fly stocks and husbandry**

520 Fly lines used in our experiments were listed in a separate table. All crosses were
521 performed at 25°C, unless stated otherwise.

522

523 **Antibody staining and confocal microscopy**

524 Antibodies used in our experiments were listed in a separate table. Embryos were
525 collected on grape juice-agar plates and processed for immunofluorescence using
526 standard procedures. Briefly, embryos were dechorionated in 50% bleach, fixed in 1:1
527 heptane:formaldehyde for 40 min and devitellinized with 80% EtOH, then stained with
528 primary and secondary antibodies in PBSTB (1X PBS, 0.1% Triton X-100, 0.2% BSA).

529 For acetylated α-tubulin, tyrosinated α-tubulin, sqh-GFP, Rok-GFP, Fog and phalloidin
530 staining, embryos were hand-devitellinized. All images were taken with a Leica SP8
531 confocal microscope.

532

533 **Cell segmentation and apical area quantification**

534 Embryos immunostained with E-Cad and CrebA were imaged using a Leica SP8 confocal
535 microscope. As Rok accumulation, apicomedial myosin and apical constriction depend
536 on the depth of invagination in the SG, SGs that were invaginated within the range of 5.1-
537 9.9 μm depth were used for quantification for proper comparison between different
538 genotypes. Maximum intensity projection was generated from three apical focal planes
539 with highest E-Cad signals for all genotypes (0.3 μm apart for each focal plane). Cells
540 were segmented along E-Cad signals and cell areas were calculated using the Imaris
541 Program (Bitplane). Since the Imaris Program calculated the areas of both the front and
542 the back of the projected cell layer, we divided the measured areas by two to get the true
543 values of apical areas of SG cells.

544

545 **Negative correlation between apical area and Rab11/Nuf intensity**

546 Cell segmentation for five WT SGs within the range of 5.1- 9.9 μm invagination was
547 performed as described above. All experiments were carried out in the same condition
548 and same settings for confocal imaging were used. Three confocal sections in the apical
549 region that show strongest Rab11/Nuf signals were used to produce the maximum
550 intensity projection. Intensity mean was measured for Rab11/Nuf signals for each
551 segmented cell using the Imaris Program (Bitplane) and plotted. Correlation (Pearson)
552 and P values were calculated using the GraphPad Prism software.

553

554 **Total intensity of Rab11, Nuf and Fog signals**

555 For measuring the total intensity of Rab11/Nuf signals in the apical region of cells in the
556 whole SG placode, the integrated density of Rab11/Nuf of each SG cell was calculated
557 (integrated density= intensity mean x area). Intensity means and SG cell areas were
558 measured using the Imaris software. The total intensity was calculated as the sum of
559 integrated densities of all cells in the placode. Five SGs were used for quantification. P
560 values were calculated using Welch's t-test in the GraphPad Prism software.

561 For the total intensity of Fog signals, background corrections were carried out first. Using
562 the Fiji software, mean gray values of Fog signals of 10 epidermal cells outside of the SG
563 placode were measured. The background intensity was calculated as the average value
564 of the intensity means of those 10 cells. The intensity mean of Fog signals of all SG cells
565 were measured using the Imaris program, and the background intensity was subtracted.
566 After background correction, the intensity mean was multiplied by SG cell areas to
567 calculate the total Fog intensity. Five SGs were used for quantification. P values were
568 calculated using Welch's t-test in the GraphPad Prism software.

569

570 **Coefficient of variation for Rab11, Nuf and Fog signals**

571 Coefficient of variation was calculated as the ratio of deviation of Rab11/Nuf intensity to
572 the mean Rab11/Nuf intensity. The mean value of Rab11/Nuf intensity was calculated as
573 the average mean intensity of Rab11/Nuf signals in all SG cells. Deviation of Rab11/Nuf
574 intensity is the difference between the mean intensity of Rab11/Nuf in each cell and the
575 mean value. Five WT SGs (690 cells) and five spastin-overexpressed SGs (496 cells)
576 were analyzed and plotted. P values were calculated using the Mann-Whitney U test in
577 the GraphPad Prism software.

578 Coefficient of variation for Fog signals of control, spastin-overexpressing and Rab11 RNAi
579 SGs were calculated using the same methods as for Rab11/Nuf. Five SGs for each
580 genotype were analyzed (control (*fkh-Gal4/*+), 475 cells; *fkh-Gal4/UAS-Spastin*, 507
581 cells; *fkh-Gal4/UAS-Rab11* RNAi, 487 cells).

582

583 **Quantification of intensities of myosin, Crb and E-Cad**

584 For myosin quantification, maximum intensity projections that span the apical and the
585 junctional region of SG cells were used (Leica LasX) and measurements were performed
586 using the Fiji software. Five SGs were used for quantification for each genotype. A group
587 of 20 cells in the dorsal/posterior region of the SG placode near the invagination pit was
588 selected for quantification of myosin intensity. Regions were drawn manually along the
589 inner or outer boundary of E-Cad signals of each cell to calculate the mean gray value of
590 apicomedial and junctional myosin.

591 For background correction, mean gray values of apicomedial myosin in ten cells outside
592 of the SG placode was measured. The average value of mean gray values of apicomedial
593 myosin in these ten cells was used to subtract the background of the cells inside the
594 placode from the same embryo. The mean intensity of apicomedial/junctional myosin was
595 normalized by the median deviation. SuperPlots (Lord et al., 2020) were used to display
596 quantification. For myosin intensity, each dot in the graph represents the average value
597 of 20 cells in each SG. For Crb and E-Cad intensities, each dot in the graph represents
598 the average value of 10 cells for each SG. Five SGs were used for quantification of all
599 three proteins. P values were calculated using Welch's t-test in the GraphPad Prism
600 software.

601

602 **Quantification of area of Rok-GFP and apicomedial myosin puncta**

603 For quantification of area of Rok-GFP puncta, a single confocal section that had the
604 strongest medial Rok signals was selected. Cell boundaries were labeled by
605 immunostaining with the antibody against E-Cad. To analyze Rok distribution, we
606 performed Particle Analysis using the Fiji software. 15 cells in the dorsal/posterior region
607 near the invagination pit were selected for quantification. Rok-GFP signals were
608 converted into black-and-white using the *Threshold* tool in Photoshop before analysis.
609 Using the *Analyze particles* tool in Fiji, Rok-GFP puncta with areas equal or larger than

610 0.02 μm^2 were measured. Five SGs were used for quantification. P values were
611 calculated using Welch's t-test in the GraphPad Prism software.

612 For measuring areas of apicomedial myosin puncta, a single confocal section with
613 strongest apicomedial myosin signals was selected. A group of 10 cells in the
614 dorsal/posterior region of SG was analyzed. Junctional myosin was excluded manually
615 and only apicomedial myosin signals were used for quantification. Measuring the area of
616 apicomedial myosin were carried out with the same method used for quantifying the area
617 of Rok-GFP puncta. Five SGs were used for quantification. P values were calculated
618 using Welch's t-test in the GraphPad Prism software.

619

620 **Quantification of length and number of gaps of junctional Crb**

621 Length of gaps and junctional length were measured using the Fiji software. Gaps that
622 have the length equal or more than 0.2 μm were quantified. If there were more than one
623 gap per junction, the length of gaps was calculated as a sum of all gaps in a given junction.
624 For each SG, 10 cells in the dorsal/posterior region were used for quantification. For the
625 number of gaps, the total number of gaps in those 10 cells were counted. Five SGs (~110
626 junctions) were used for quantification. P values were calculated using Welch's t-test in
627 the GraphPad Prism software.
628

Fly strains	**Source**	**RRID**	**References**
Rab11-EYFP	Bloomington Stock Center	62549	(Dunst et al., 2015)
Rab5-EYFP	Bloomington Stock Center	62543	(Dunst et al., 2015)
Rab7-EYFP	Bloomington Stock Center	62545	(Dunst et al., 2015)
UAS-Spastin (on II)	N. Sherwood, Duke		(Sherwood et al., 2004)
UAS-Spastin-CFP (on III)	N. Sherwood, Duke		(Du et al., 2010)
fkh-Gal4 (on II)	D. Andrew (John Hopkins University)		(Chung et al., 2017)
fkh-Gal4 (on III)	D. Andrew (John Hopkins University)		(Chung et al., 2017)
ubi-Rok-GFP	S. Parkhurst (Fred Hutchinson Cancer Research Center)		(Abreu-Blanco et al., 2014)
sqh-GFP			(Royou et al., 2004)

UAS-Rab11S25N-EYFP	Bloomington Stock Center	9792, 23261	
UAS-Dicer-2	Bloomington Stock Center	60008	
UAS-Dhc64C RNAi	Bloomington Stock Center Vienna *Drosophila* Resource Center	76941, 28749, v28053, v28054. 4 lines worked equally. v28054 was used for all of the data shown in this work.	
klar^{1}	Bloomington Stock Center	3256	
klar^{mCD4}	Bloomington Stock Center	25097	
klar^{mCD4} *ubi-Rok-GFP*	Recombinant line generated from *klar*^{mCD4} and *ubi-Rok-GFP*		
UAS-Crb RNAi	Bloomington Stock Center	38373, 38903, 40869, 34999.	

		4 lines worked equally. 2 lines (38373, 34999) were used for the data shown in this work.	
UAS-E-Cad RNAi	Bloomington Stock Center	32904	
UAS-Shg-GFP	Bloomington Stock Center	58445	
UAS-Rab11 RNAi	Bloomington Stock Center	42709, 27730. Line 42709 was used for testing myosin and Rok-GFP signals. Line 27730 was used for the rest of the experiments.	

629

630

Antibody	Source	RRID	Dilution
α-E-Cad (rat)	DSHB (deposited by T. Uemura, Kyoto University)	DCAD2 (AB_528120)	1:50
α-CrebA (rat)	Andrew lab (John Hopkins University)		1:3000
α-CrebA (rabbit)	Andrew lab (John Hopkins University)		1:5000
α-Dhc (mouse)	DSHB (deposited by J.M. Scholey, University of California)	2C11-2 (AB_2091523)	1:50
α-Rab11 (rabbit)	Andrew lab (John Hopkins University)		1:500
α-Nuf (guinea pig)	Sotillos lab (CABD)		1:500
α-acetylated α-tubulin (mouse)	Invitrogen	32-2700 (AB_2533073)	1:1000
α-tyrosinated α-tubulin (rat)	Invitrogen	MA1-80017 (AB_2210201)	1:1000
α-GFP (chicken)	Invitrogen	A10262 (AB_2534023)	1:500

α-β-galactosidase (rabbit)	Invitrogen	A11132 (AB_221539)	1:500
α-Crb (mouse)	DSHB (deposited by E. Knust, Max Planck Institute)	Cq4 (AB_528181)	1:10
α-Fog (rabbit)	N. Fuse (Fuse et al., 2013)		1:1000
α-Sec15 (guinea pig)	Bellen lab (Baylor College of Medicine)		1:2000
Alexa Fluor 488/568/647-coupled secondary antibodies	Invitrogen		1:500

631

632 **Acknowledgments**

633 We thank the members of the Chung laboratory for comments and suggestions. We thank
634 A. Martin, S. Parkhurst and N. Sherwood and the Bloomington stock center for fly stocks,
635 and D. Andrew, H. Bellen, S. Sotillos and the Developmental Studies Hybridoma Bank
636 for antibodies. We thank Flybase for the gene information. We are grateful to A. Bohnert,
637 C. Hanlon, A. Johnson and C. O'Kane for their helpful comments on the manuscript. This
638 work is supported by start-up fund from Louisiana State University and the grant from the
639 Board of Regents Research Competitiveness Subprogram GR-00005224 to S.C.
640

641 **Figure legends**

642 **Figure 1. Intracellular trafficking components are apically enriched in invaginating**
643 **SGs.** (A) A schematic drawing of the anterior region of the *Drosophila* embryo for stage
644 11 (ventral and lateral views) and stage 16 (lateral view) with SGs shown in green. Top
645 right, magnified view of a stage 11 SG. The region where SG cells undergo clustered
646 apical constriction during invagination is shown in purple. (B-B'') En face (top) and lateral
647 (bottom) views of a wild type stage 11 SG immunostained for E-Cad, Rab11 and Nuf.
648 Rab11 and Nuf show apical enrichment near the invagination pit (yellow arrowheads).
649 Red arrowheads, Rab11 and Nuf signals near the segmental groove. (B'''-B''''') Heat
650 maps of apical area (B''') and intensity of Rab11 (B'''') and Nuf (B'''''). Cells with smaller
651 apical areas near the invagination pit (dark blue cells in B''') show high intensity of Rab11
652 and Nuf (red signals in B'''' and B'''''). (C-C''') En face (top) and lateral (bottom) views of
653 a wild type stage 11 SG immunostained for E-Cad (C) and Dhc64C (C'). Corresponding
654 heat maps for apical areas (C'') and intensity of Dhc64C signals (C''') are shown. (D-F''')
655 Wild type stage 11 SGs immunostained for E-Cad and Rab11 at different timepoints of
656 invagination. (G) Total intensity of Rab11 in the whole SG placode before and during
657 invagination. Before invagination, n= 4 SGs; during invagination, n= 5 SGs. (H) Negative
658 correlation between Rab11 intensities and apical areas of SG cells before (top) and during
659 invagination (bottom). R, Pearson correlation coefficient. $p < 0.0001$ for all samples.
660 Before invagination, n= 4 SGs, 506 cells; during invagination, n= 4 SGs, 561 cells.
661 Asterisks: invagination pit. White lines: SG boundary. SG boundaries are marked based
662 on CrebA (SG nuclear marker) signals in the basal region of SG cells (not shown).

663

664

Figure 1

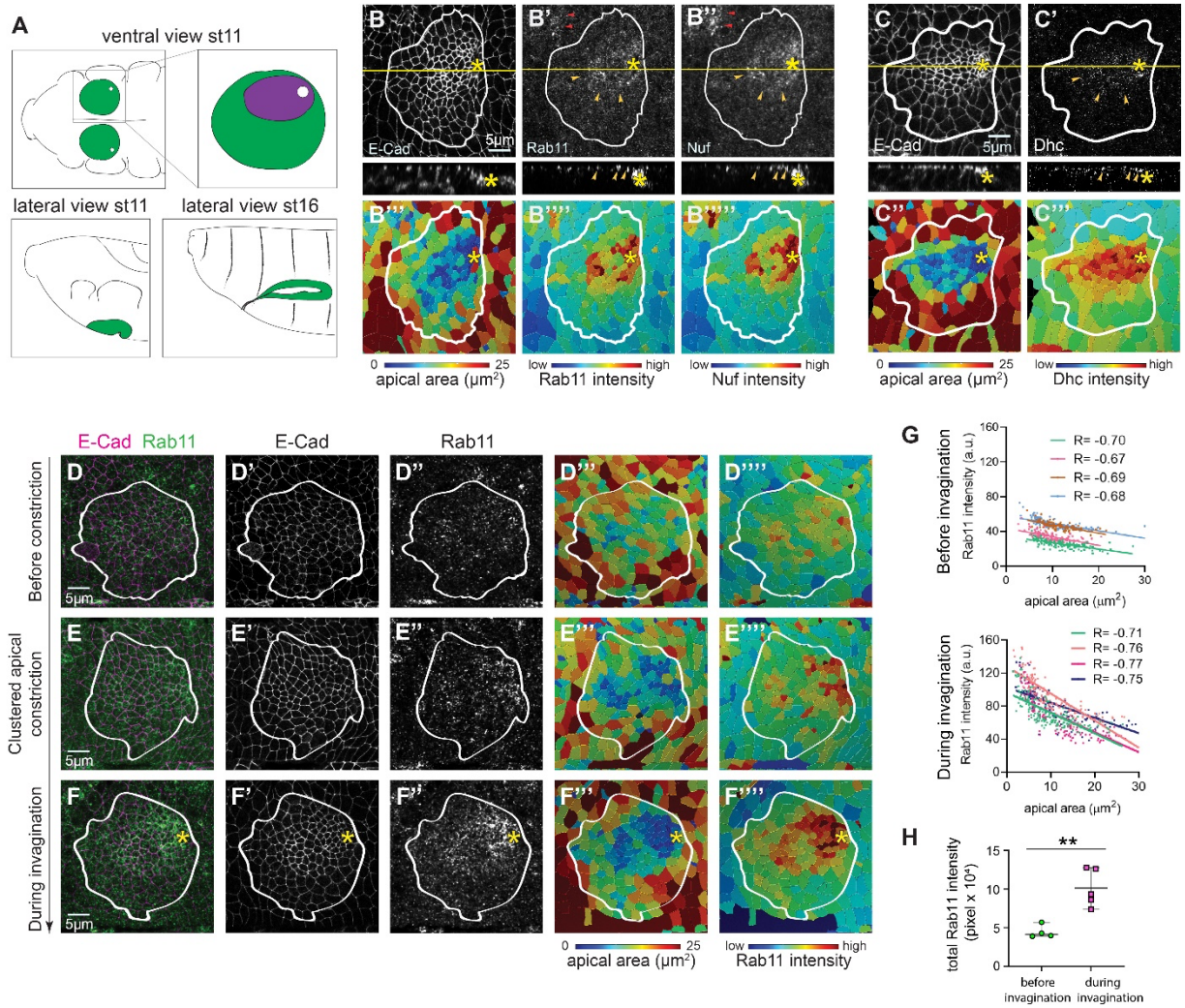

665

666

667 **Figure 2. Disruption of MTs results in mislocalization of Rab11 and Nuf to the**
668 **basolateral domain in SG cells.** (A-A’’’) A wild type SG immunostained for Rab11
669 (green) and tyrosinated α-tubulin (Tyr-α-Tub; purple). Higher magnification of the yellow
670 boxed area is shown in A’-A’’’. Yellow arrowheads, co-localized Rab11 and tyrosinated
671 α-tubulin. (B-B’’) Z sections along the yellow line in A. (C-C’’’) En face (top) and lateral
672 (bottom) views of a control (*fkh-Gal4/*+) SG show abundant levels of tyrosinated α-tubulin
673 (C’’; Tyr-α-Tub) and acetylated α-tubulin (C’’’; Ace-α-Tub). (D-D’’’) Overexpression of
674 spastin in the SG using *fkh-Gal4* leads to reduction of tyrosinated α-tubulin (D’’) and loss
675 of acetylated α-tubulin (D’’’). Whereas Rab11 is enriched in the apical domain of WT SG
676 cells (yellow arrowheads in C’), Rab11 mislocalizes basolaterally when spastin is
677 overexpressed (red arrowheads in D’). (E-F’’) Confocal images of WT (E and E’) and
678 spastin-overexpressing SGs (F, F’) stained for Rab11 (E, F) and Nuf (E’, F’). Maximum
679 projection of three confocal sections for the apical domain is shown. Compared to strong
680 Rab11 and Nuf signals in the apical domain in WT SGs (yellow arrowheads in E and E’),
681 Rab11 and Nuf are reduced in spastin-overexpressing SGs (red arrowheads in F and F’).
682 (G) Total intensity of Rab11 and Nuf in the whole SG placode in control and spastin-
683 overexpressing SG. n= 5 SGs for each genotype. (H) Coefficient of variation of Rab11
684 (left) and Nuf (right) intensities in the SG (n= 5 SGs for both genotypes; WT, 690 cells;
685 *fkh-Gal4/UAS-Spastin*, 496 cells). ****, $p<0.0001$, Mann-Whitney U test. Asterisks:
686 invagination pit. White lines: SG boundary.

687

688

Figure 2

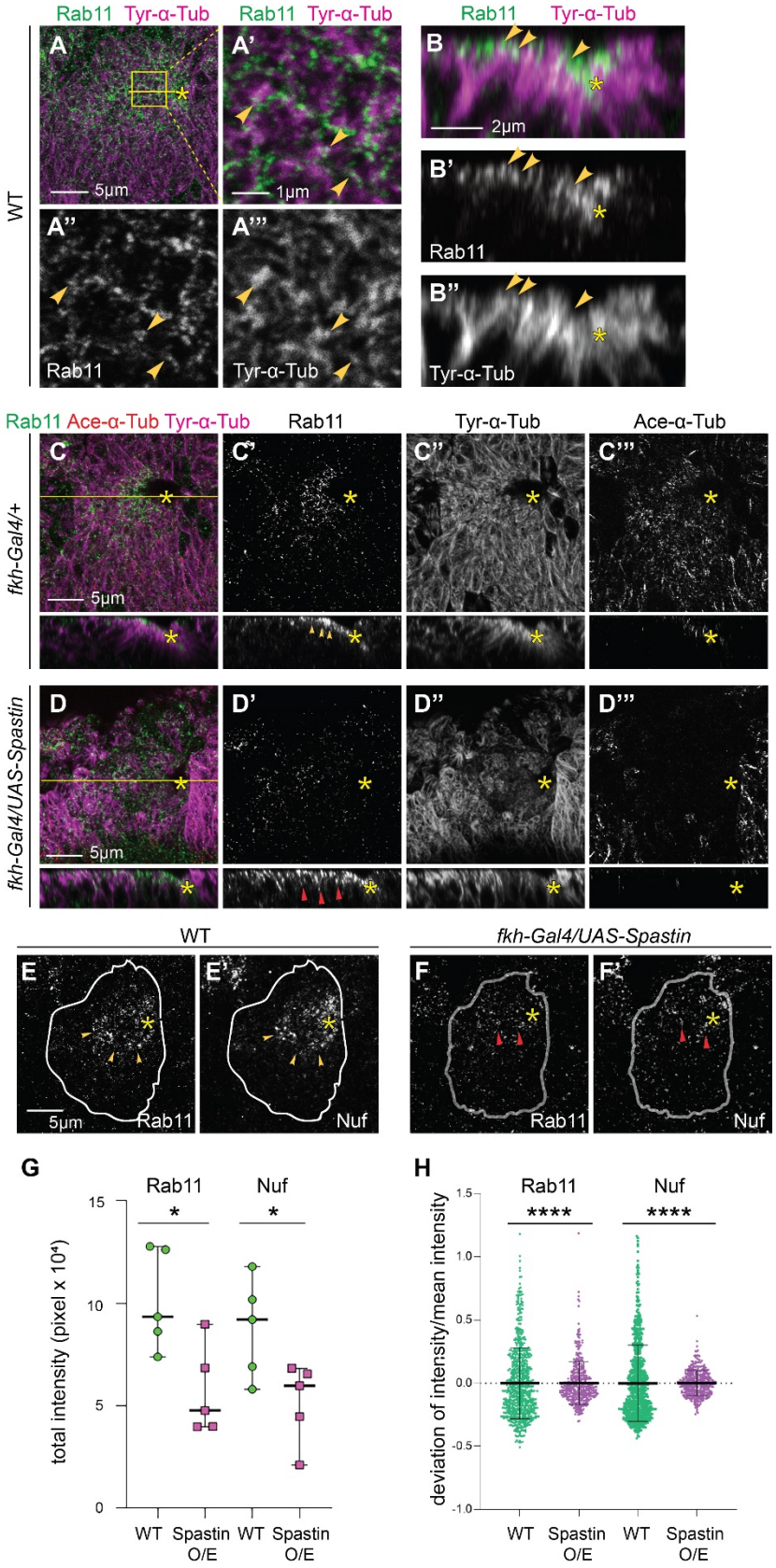
Rab11 Tyr-α-Tub
Rab11 Tyr-α-Tub
Rab11 Tyr-α-Tub
WT
A
A'
B
5μm
1μm
2μm
A''
A'''
B'
B''
Rab11
Tyr-α-Tub
Rab11
Tyr-α-Tub
Rab11 Ace-α-Tub Tyr-α-Tub
Rab11
Tyr-α-Tub
Ace-α-Tub
fkh-Gal4/+
C
C'
C''
C'''
5μm
fkh-Gal4/UAS-Spastin
D
D'
D''
D'''
5μm
WT
fkh-Gal4/UAS-Spastin
E
E'
F
F'
5μm
Rab11
Nuf
Rab11
Nuf
G
Rab11
Nuf
*
*
total intensity (pixel x 10⁴)
15
10
5
0
WT
Spastin O/E
WT
Spastin O/E
H
Rab11
Nuf
****
****
deviation of intensity/mean intensity
1.5
1.0
0.5
0.0
-0.5
-1.0
WT
Spastin O/E
WT
Spastin O/E

689

690 **Figure 3. Rab11 and dynein functions are required for coordinated apical**
691 **constriction in the SG.** (A-F) Confocal images of control (A), Rab11-DN-overexpressing
692 (B), *Rab11* RNAi (C), *Dhc64C* RNAi (D), wild type (E) and *klar* mutant (F) SGs
693 immunostained for E-Cad. (A'-F') Heat maps corresponding to images shown in A-F. (G,
694 H) Percentage (G) and cumulative percentage (H) of SG cells with different apical areas.
695 Mann-Whitney U test (for percentage of cells) and Kolmogorov-Smirnov test (for
696 cumulative percentage of cells). n= 5 SGs (control (*fkh-Gal4/*+), 517 cells; *fkh>Rab11-*
697 *DN*, 536 cells; *fkh>Rab11* RNAi, 474 cells; *fkh>Dhc64C* RNAi, 499 cells) and 6 SGs (WT,
698 690 cells; $klar^1$, 705 cells). *, $p<0.05$; ****, $p<0.0001$. (I-J'') Control (I-I'') and *Dhc64C* RNAi
699 (J-J'') SGs stained for tyrosinated-α-Tub (I', J') and phalloidin (I'', J''). Compared to control
700 (I'), tyrosinated-α-Tub (Tyr-α-Tub) is decreased in *Dhc64C* RNAi SGs (J'). (I-J'') WT (K-
701 K'') and *klar* mutant (L-L'') SGs stained for acetylated-α-Tub (Ace-α-Tub; K', K') and
702 phalloidin (L'', L''). No significant changes in acetylated-α-Tub levels are detected in *klar*
703 mutant SGs. Asterisks: invagination pit. White lines: SG boundary.

Figure 3

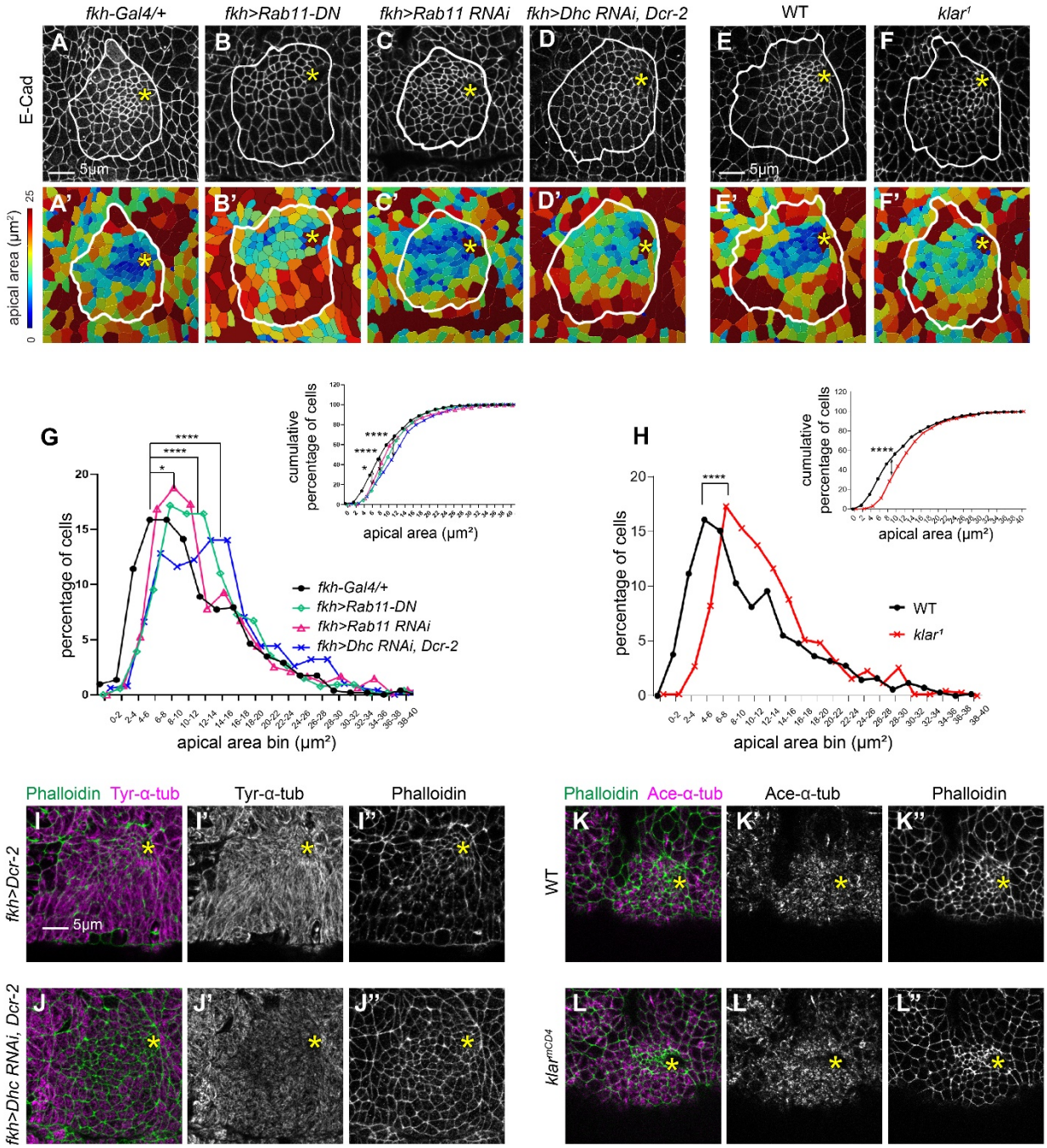

704

705

706 **Figure 4. Compromised Rab11 functions lead to a reduction of apicomedial myosin**
707 **formation and impairs apicomedial Rok accumulation in SG cells.** (A-B’’’) sqh-GFP
708 signals in control (A-A’’’) and *Rab11* RNAi (B-B’’’) SGs immunostained for E-Cad and
709 GFP. Higher magnification of the yellow boxed area in A and B are shown in A’’-A’’’ and
710 B’’-B’’’. Compared to strong signals of apicomedial myosin web structures in the control
711 SG (yellow arrowheads in A’’), reduced and dispersed myosin signals are detected upon
712 *Rab11* knockdown (red arrowheads in B’’). (A’’’’ and B’’’’) Inverted sqh-GFP signals are
713 used for measuring areas of apicomedial myosin structures. (C-E) Quantification of the
714 intensity of apicomedial (AM) and junctional (J) myosin (C), the ratio of apicomedial to
715 junctional myosin (D) and areas of apicomedial myosin (E) in control and *Rab11* RNAi
716 SG cells. n= 5 SGs for both genotypes; 10 cells in the dorsal/posterior region of each SG.
717 *, $p< 0.05$; **, $p< 0.01$. Welch’s t-test. (F-G’’) Rok-GFP signals in control (F, F’) and Rab11
718 RNAi (G, G’) SGs immunostained for E-Cad and GFP. Higher magnification of the yellow
719 boxed area in F and G are shown in F’ and G’. Compared to strong accumulation of Rok-
720 GFP signals in the apicomedial region of control SG cells (yellow arrowheads in F’), Rok-
721 GFP signals are more dispersed when *Rab11* is knocked down (red arrowheads in G’).
722 (F’’ and G’’) Inverted Rok-GFP signals are used for measuring areas of apicomedial Rok
723 accumulation. (H) Quantification of areas of Rok-GFP puncta. *, $p< 0.05$; **, $p<0.01$.
724 Welch’s t-test. n= 5 SGs for all genotypes; 15 cells in the dorsal/posterior region for each
725 SG. Asterisks: invagination pit.

Figure 4

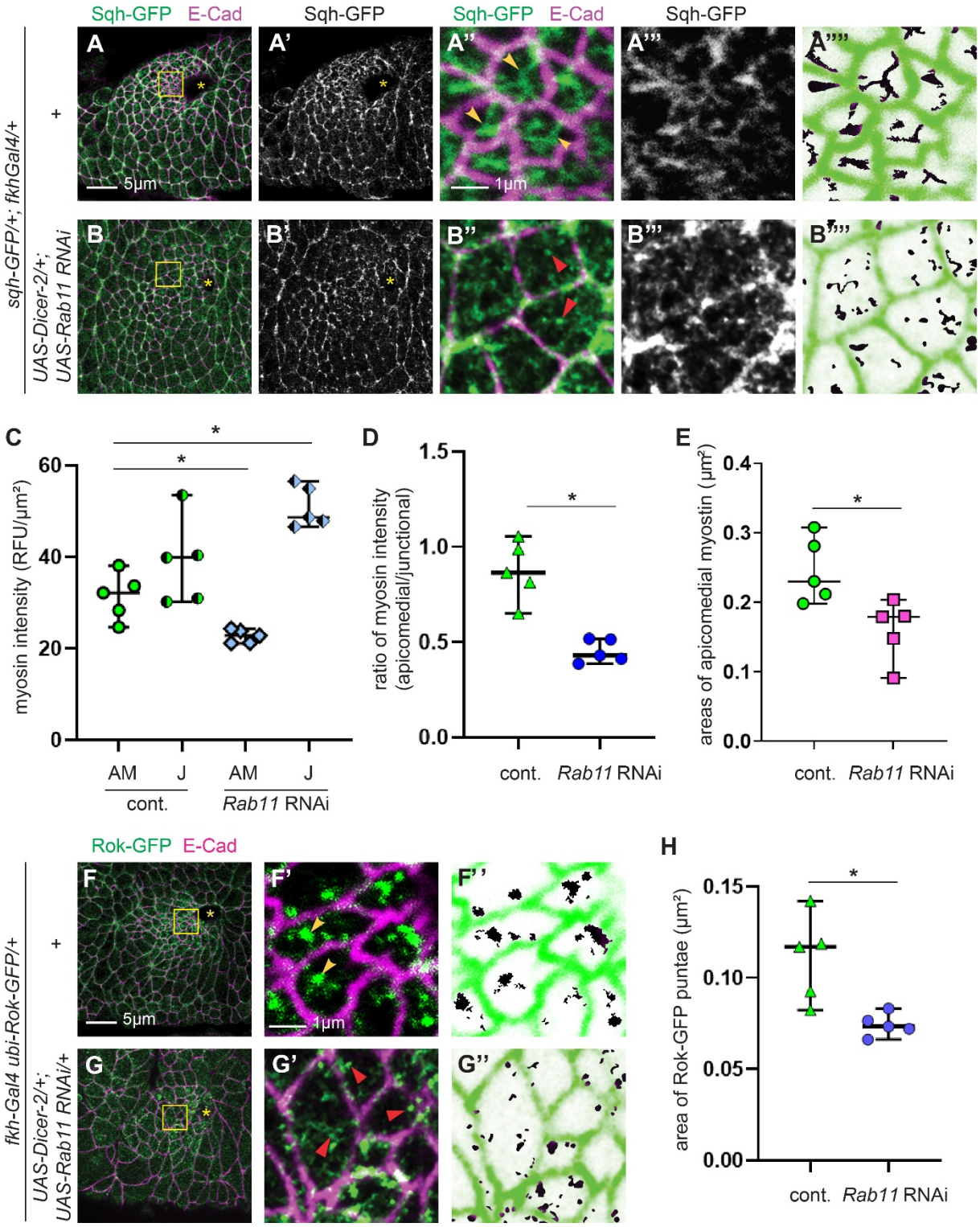
Sqh-GFP E-Cad
Sqh-GFP
Sqh-GFP E-Cad
Sqh-GFP
A
A'
A''
A'''
A''''
B
B'
B''
B'''
B''''
5µm
1µm
sqh-GFP/+; fkhGal4/+
+
UAS-Dicer-2/+;
UAS-Rab11 RNAi
C
myosin intensity (RFU/µm²)
AM
J
AM
J
cont.
Rab11 RNAi
D
ratio of myosin intensity (apicomedial/junctional)
cont.
Rab11 RNAi
E
areas of apicomedial myostin (µm²)
cont.
Rab11 RNAi
Rok-GFP E-Cad
F
F'
F''
G
G'
G''
fkh-Gal4 ubi-Rok-GFP/+
UAS-Dicer-2/+;
UAS-Rab11 RNAi/+
H
area of Rok-GFP puntae (µm²)
cont.
Rab11 RNAi

728 **Figure 5. Compromised dynein function leads to a reduction of apicomedial myosin**
729 **formation and impairs apicomedial Rok accumulation in SG cells.** (A-B', F-G') sqh-
730 GFP signals in control (A, A', F, F'), *Dhc64C* RNAi (B, B') and *klar* mutant (G, G') SGs
731 immunostained for E-Cad and GFP. Higher magnification of the yellow boxed area in A,
732 B, F and G are shown in A', B', F' and G'. Yellow and red arrowheads indicate apicomedial
733 myosin. (C-E, H-J) Quantification of the intensity of apicomedial and junctional myosin
734 (C, H), the ratio of apicomedial to junctional myosin (D, I) and areas of apicomedial myosin
735 (E, J) in SG cells. n= 5 SGs for all genotypes; 10 cells in the dorsal/posterior region of
736 each SG. *, $p< 0.05$; **, $p< 0.01$, Welch's t-test. (A-A'') (K-O') Rok-GFP signals in control
737 (K, K', N, N'), spastin-overexpressing (L, L'), *Dhc64C* RNAi (M, M') and *klar* mutant (O,
738 O') SGs immunostained for E-Cad and GFP. Higher magnification of the yellow boxed
739 area in K-O are shown in K'-O'. (P, Q) Quantification of areas of Rok-GFP puncta. *, $p<$
740 0.05; **, $P<0.01$, Welch's t-test. n= 5 SGs for all genotypes; 15 cells in the dorsal/posterior
741 region for each SG. Asterisks: invagination pit.

Figure 5

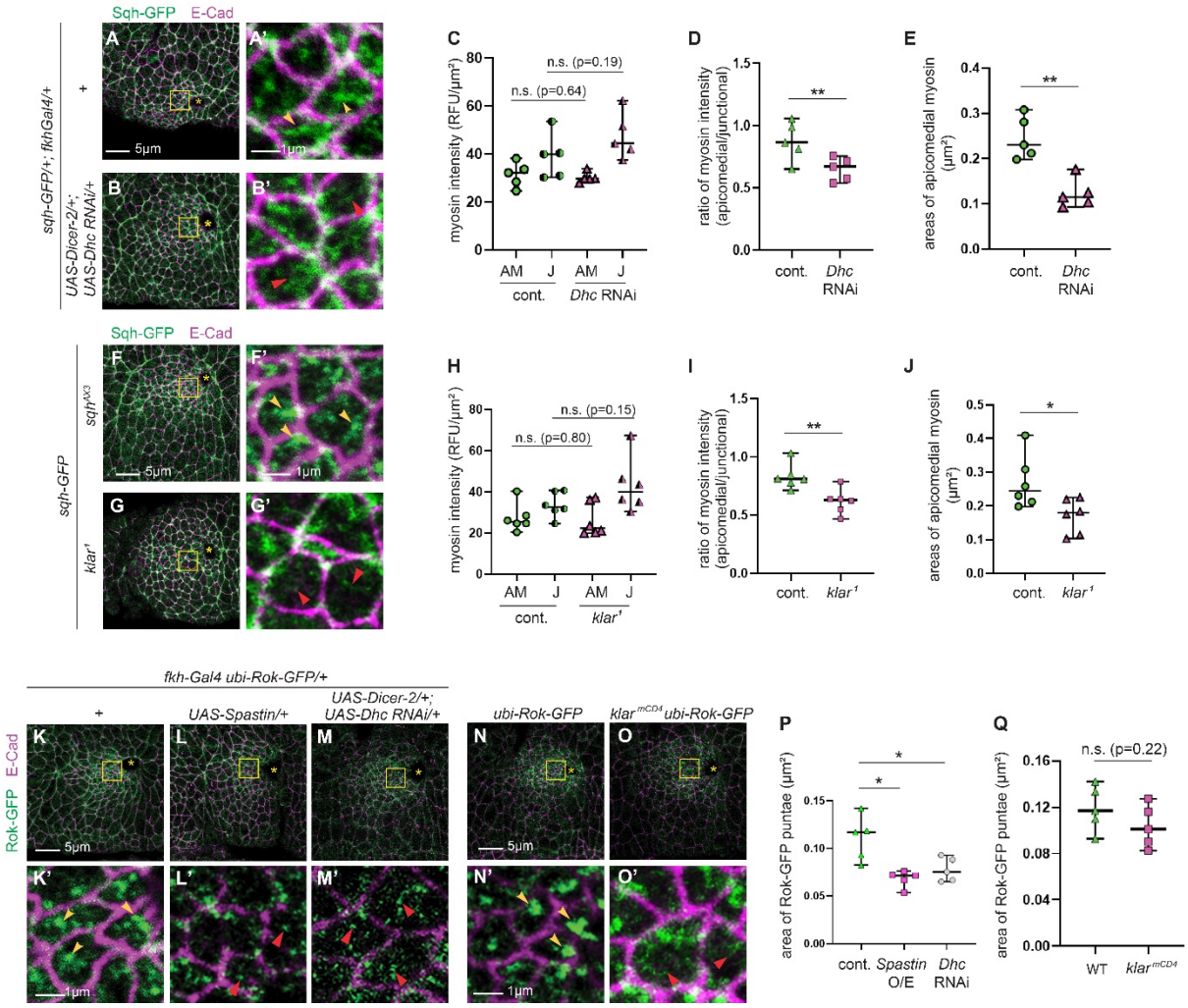

742

743

744 **Figure 6. MTs and Rab11 are required for apical transport of Fog, Crb and E-Cad**
745 **during SG invagination.** (A-C') Confocal images for control (A-A'), spastin-
746 overexpressing (B-B') and *Rab11* RNAi (C-C') SGs immunostained for E-Cad and Fog.
747 (A''-C''') Corresponding heat maps for apical area (A''-C'') and Fog intensity (A'''-C'''). (D-
748 F'''') Confocal images for control (A-A'), spastin-overexpressing (B-B') and *Rab11* RNAi
749 (C-C') SGs immunostained for E-Cad and Crb. Higher magnification of boxed areas in D-
750 F are shown in D'''-F''''. Compared to junctional enrichment of E-Cad signals in the control
751 SG (D''), E-Cad mislocalizes to the basolateral region in spastin-overexpressing (E'') and
752 *Rab11* RNAi (F'') SGs (red arrowheads). Compared to relatively continuous Crb signals
753 in the control SG (D'''), Crb signals show gaps (red arrows) in spastin-overexpressing
754 (E''') and *Rab11* RNAi (F''') SGs. (G) Total intensity of apical Fog signals in the entire SG
755 placode in control, spastin-overexpressing and *Rab11* knocked down SG. n= 5 SGs for
756 each genotype. (H) Coefficient of variation for Fog signals. n= 5 SGs (control (*fkh-Gal4/+*),
757 475 cells; *fkh-Gal4/UAS-spastin*, 507 cells; *fkh-Gal4/UAS-Rab11* RNAi, 487 cells).
758 Kolmogorov-Smirnov test. (I) Quantification of the ratio of length of gaps to junctional
759 length (Welch's t-test) in SGs immunostained for Crb. (J) Quantification of the number of
760 gaps (Welch's t-test) in SGs immunostained for Crb. n= 5 SGs; 10 cells for each SG.
761 Asterisks: invagination pit.

762

Figure 6

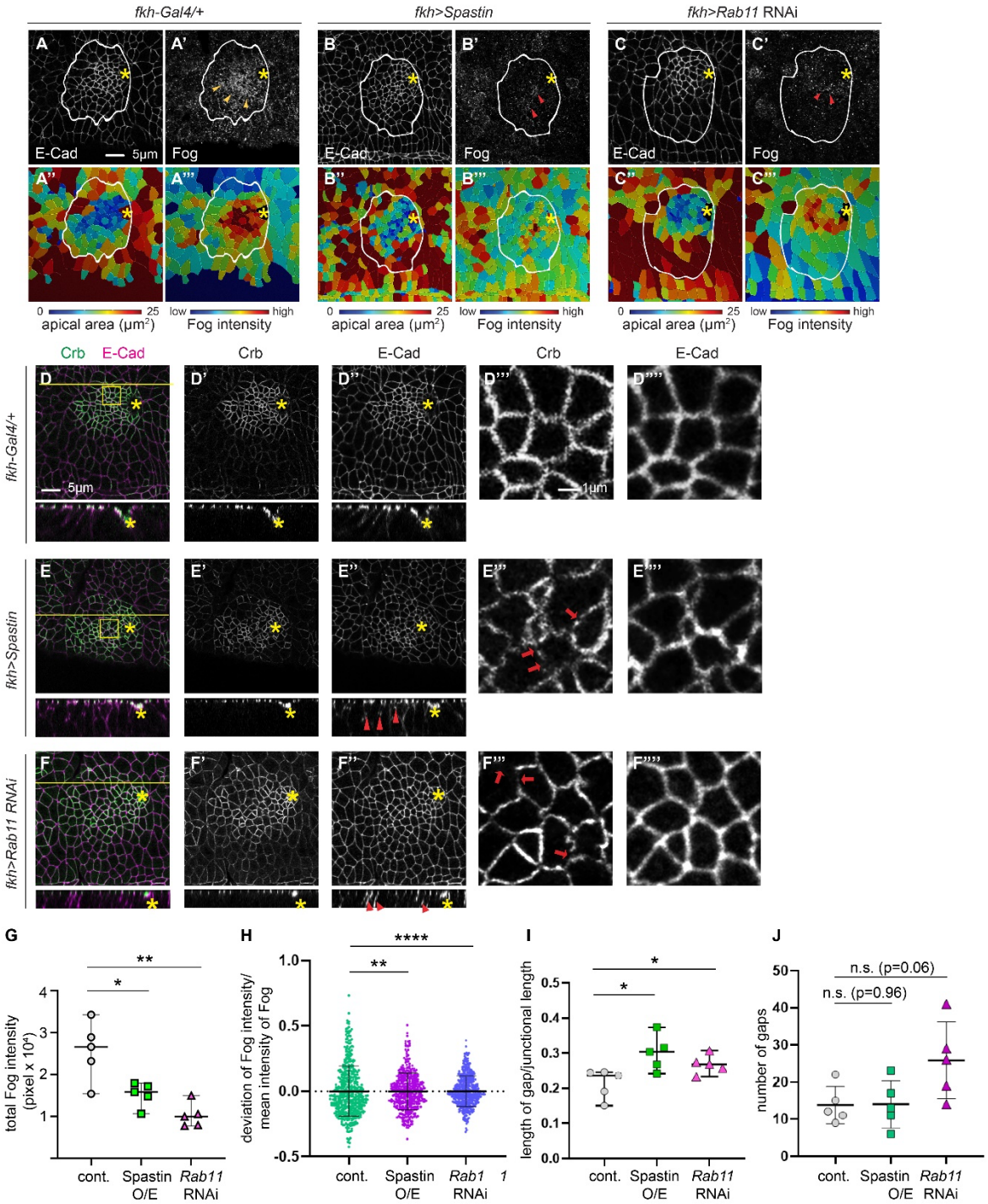

763

764

765 **Figure 7. Crb and E-Cad have roles in regulating apical constriction during SG**
766 **invagination.** (A-C) Confocal images of control (A), *crb* RNAi (B) and *E-Cad* RNAi (C)
767 SGs immunostained for E-Cad. (A'-C') Corresponding heat maps for apical areas in SGs
768 shown in A-C. (D) Percentage and cumulative percentage of cells with different apical
769 areas. Mann-Whitney U test (percentage of cells) and Kolmogorov-Smirnov test
770 (cumulative percentage of cells). n= 5 SGs (control, 517 cells; *crb* RNAi, 583 cells; *E-Cad*
771 RNAi, 712 cells). *, p<0.05; ****, p<0.0001. Asterisks: invagination pit. White lines: SG
772 boundary.

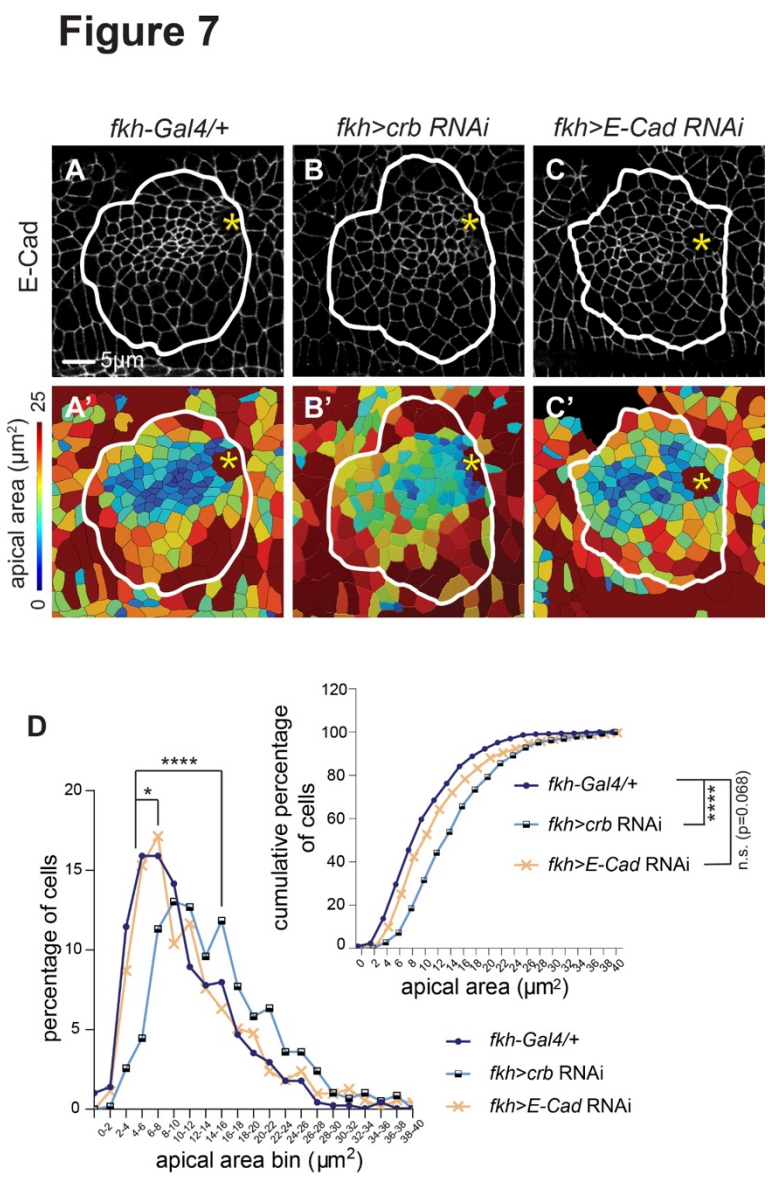

773
774

775 **Figure 8. Knockdown of *crb* or *E-Cad* results in reduced apicomedial myosin**
776 **formation and dispersed apicomedial Rok.** (A-C”) sqh-GFP signals in control (A-A’’),
777 *crb* RNAi (B-B’’) and *E-Cad* RNAi (C-C’’) SGs immunostained for E-Cad and GFP. (A”-
778 C”) Higher magnification of yellow boxed areas in A-C. (D-F”) Rok-GFP signals in control
779 (D-D’’), *crb* RNAi (E-E’’) and *E-Cad* RNAi (F-F’’) SGs immunostained for E-Cad and GFP.
780 (D”-F”) Higher magnification of yellow boxed areas in D-F. (G-I) Quantification of the
781 intensity of apicomedial and junctional myosin (G), the ratio of apicomedial to junctional
782 myosin (H) and areas of apicomedial myosin structures (I) in SG cells from different
783 genotypes shown in A-C (n=5 SGs for each genotype; 10 cells in the dorsal/ posterior
784 region). *, p<0.05; **, p<0.01. Welch’s t-test. (F-I’’) (J) Quantification of areas of Rok-GFP
785 puncta in SG cells from different genotypes shown in D-F (n=5 SGs; 15 cells in the
786 dorsal/posterior for each genotype). *, p<0.05; **, p< 0.01. Welch’s t-test. Asterisks:
787 invagination pit.

Figure 8

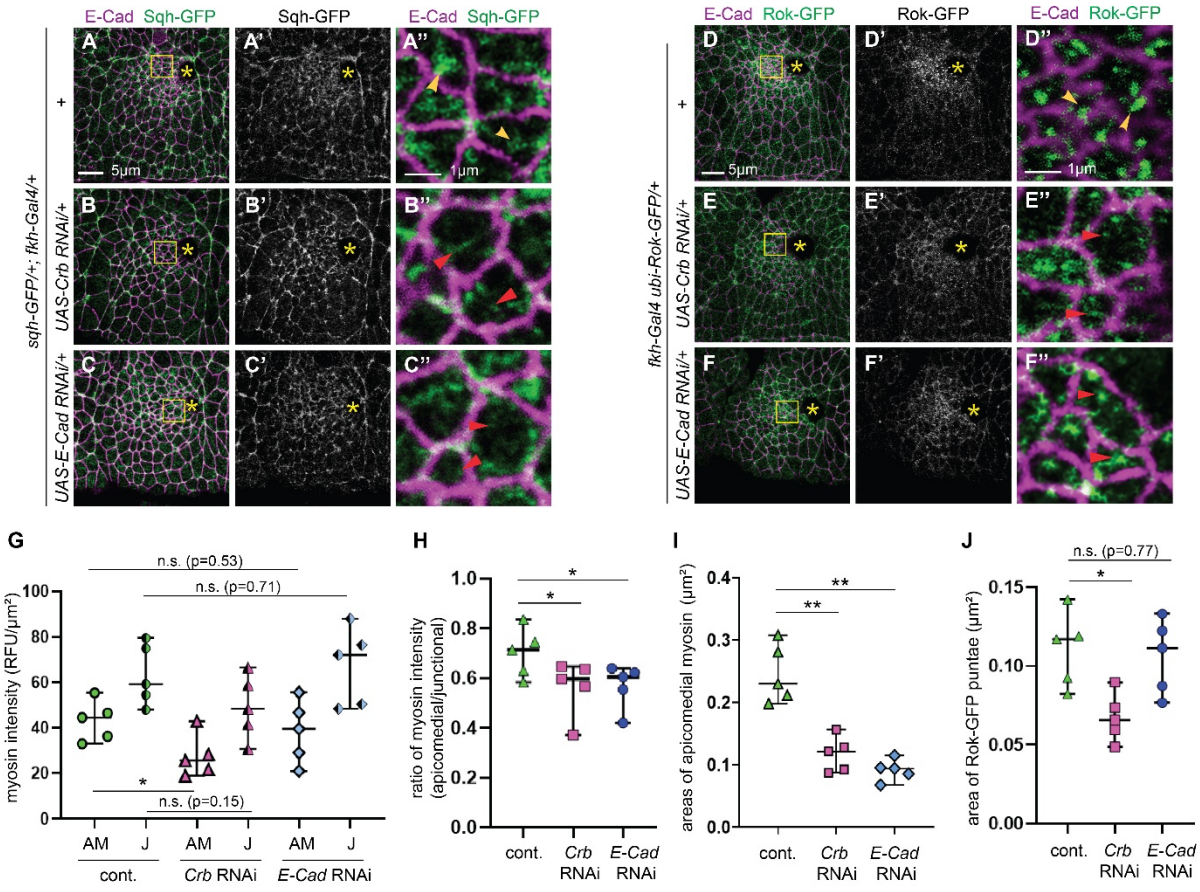

788
789

790 **Figure 9. A proposed model for MT-dependent trafficking to promote apical**
791 **constriction during SG invagination.** Vesicular transport is essential for apical
792 localization of Fog, Crb and E-Cad to regulate apical myosin networks and subsequent
793 apical constriction. Precise roles for the dynein motor in regulating apical constriction
794 remain to be determined. Red question mark represents a potential role of dynein in
795 trafficking cargos to the apical region of SG cells during apical constriction.

796

Figure 9

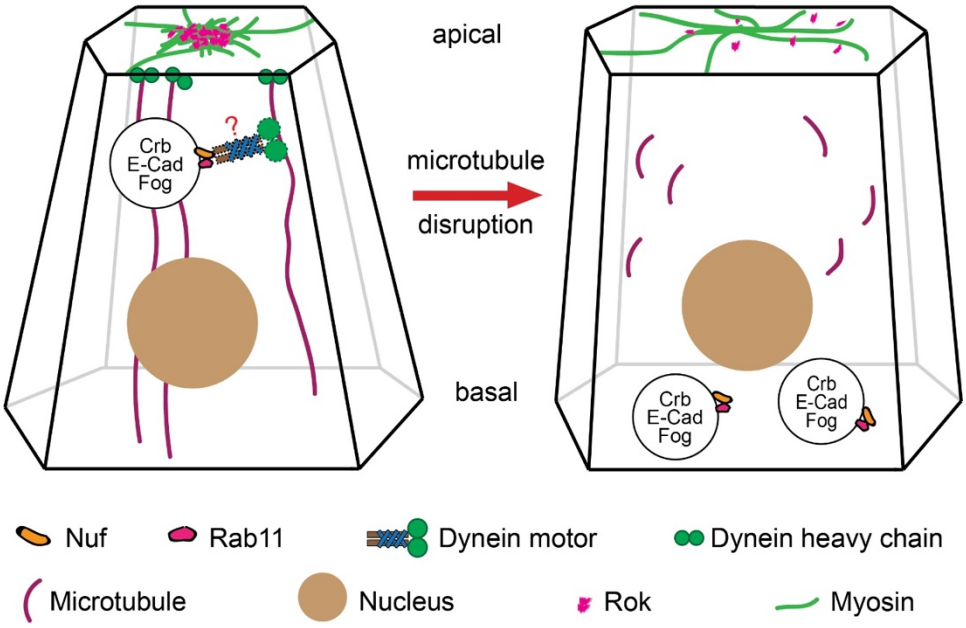

797
798

799 **Figure S1. Rab11-EYFP, Rab5-EYFP and Sec15 are apically enriched in the**
800 **invaginating SG.** (A-A'') *Rab11-EYFP* (an EYFP insertion at the N-terminus under the
801 control of Rab11 regulatory sequences) SG labeled with antibodies against E-Cad (A),
802 GFP (A') and Nuf (A''). (A'''-A''''') Corresponding heat maps for apical areas of SG cells
803 (A''') and intensities of GFP (A'''') and Nuf (A''''') signals. (B, B') Confocal images of a
804 *Rab5-EYFP* (an EYFP insertion at the N-terminus under the control of Rab5 regulatory
805 sequences) SG stained for E-Cad (B) and GFP (B'). (B'', B''') Corresponding heat maps
806 for apical areas of SG cells (B'') and intensity of Rab5-EYFP signals (B'''). (C) Negative
807 correlation between Rab5-EYFP intensity and apical areas of SG cells (n= 4 SGs; 396
808 cells). (D-D') *Rab7-EYFP* (an EYFP insertion at the N-terminus under the control of Rab7
809 regulatory sequences) SG immunostained for E-Cad (D) and GFP (D'). (D'', D''')
810 Corresponding heat maps for apical areas of SG cells (D'') and intensity of Rab7-EYFP
811 (D'''). (E-E''') Wild type SG immunostained for E-Cad (E) and Sec15 (E'). (E'', E''')
812 Corresponding heat maps for apical areas of SG cells (E'') and intensity of Sec15 signals
813 (E'''). (F) Negative correlation between intensity of Sec15 and apical areas of SG cells
814 (n= 5 SGs; 527 cells). Asterisks: invagination pit. White lines, SG boundary.

Supplemental Figure 1

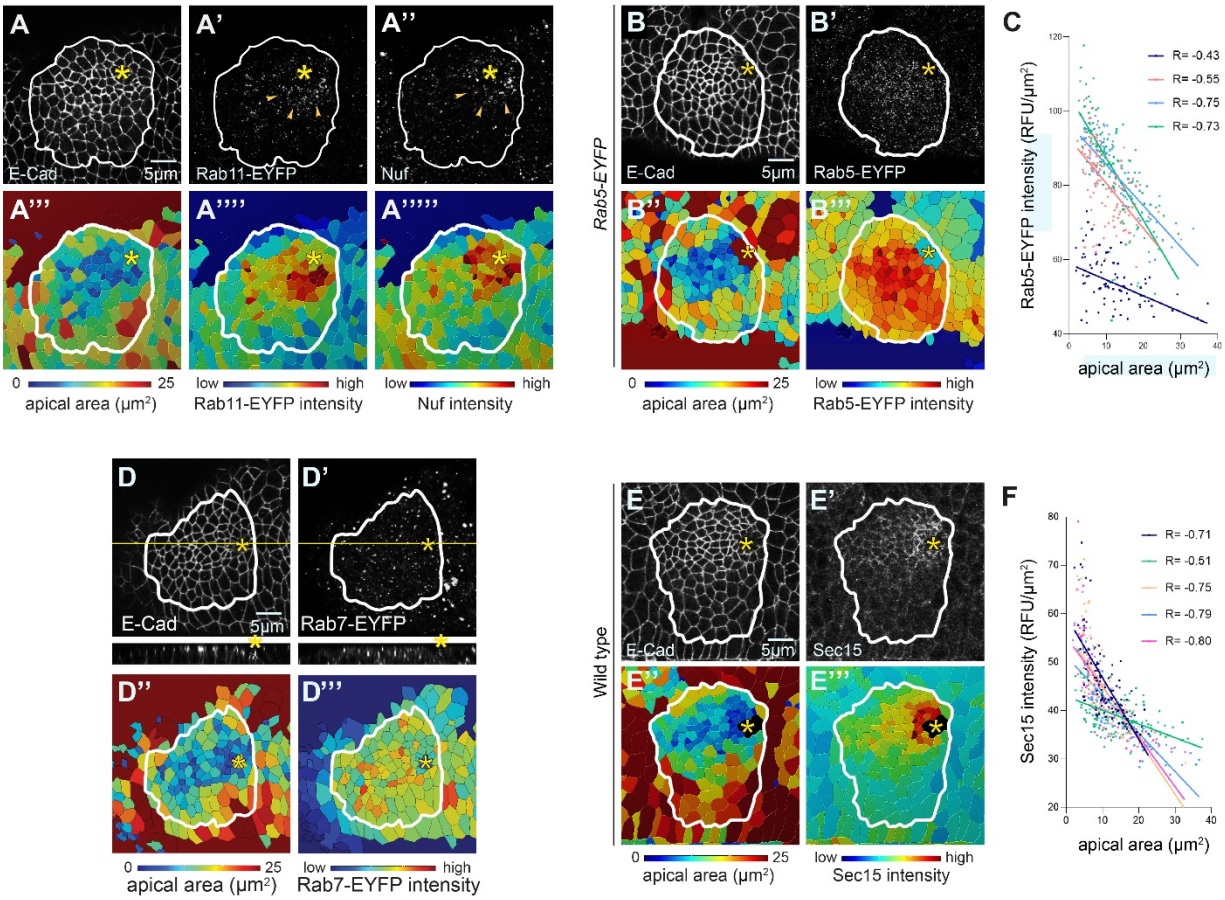

817 **Figure S2. Overexpression of spastin in the SG results in loss of acetylated-α-**
818 **tubulin.** (A-B'') Confocal images of control (A-A'') and spastin-CFP-overexpressing (B-
819 B'') SGs stained for phalloidin (red) and an antibody against acetylated α-tubulin (Ace-α-
820 Tub; magenta). Spastin-CFP (green) signals show SG-specific overexpression of spastin
821 by *fkh-Gal4*, which leads to a loss of MTs in the SG placode. Asterisks, invagination pit.

822

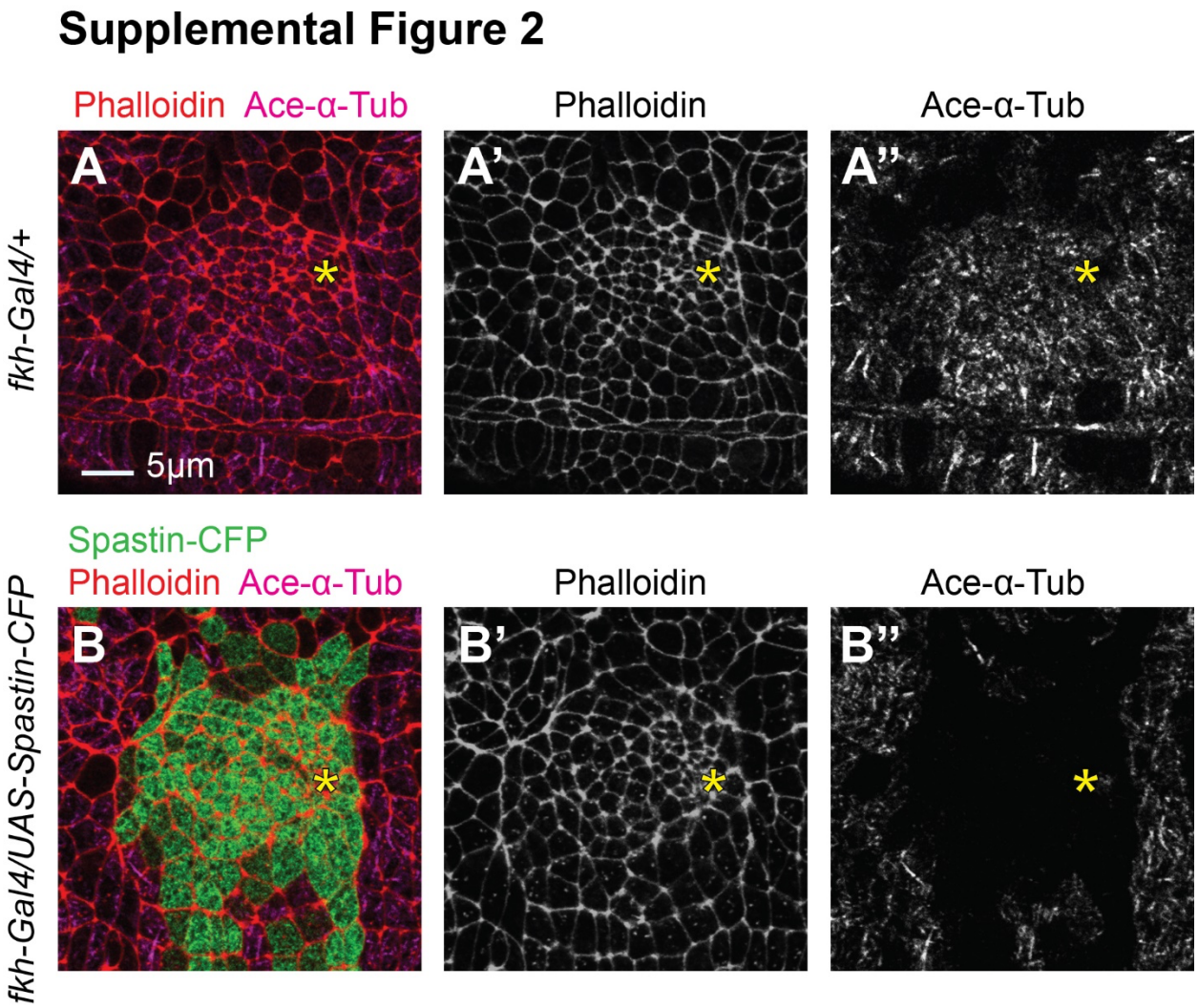

823
824

825 **Figure S3. Verification of RNAi knockdown in the SG.** (A-D') Control (A-B') and *Rab11*
826 RNAi (C-D') SGs immunostained for Sage (SG nuclei) and Rab11. Stage 11 (A, A', C, C')
827 and stage 13 (B, B', D, D') SGs are shown. (E, E') Stage 11 control (E) and *crb* RNAi (C-
828 D') SGs immunostained for Crb. (E'') Quantification of junctional intensity of Crb. (F, F')
829 Stage 11 control (E) and *E-Cad* RNAi (C-D') SGs immunostained for E-Cad. (F'')
830 Quantification of junctional intensity of E-Cad. n= 5 SGs for both in E'' and F''; 10 cells in
831 the dorsal/posterior region of each SG. **, $p < 0.01$ (Welch's t-test). Asterisks, invagination
832 pit.

Supplemental Figure 3

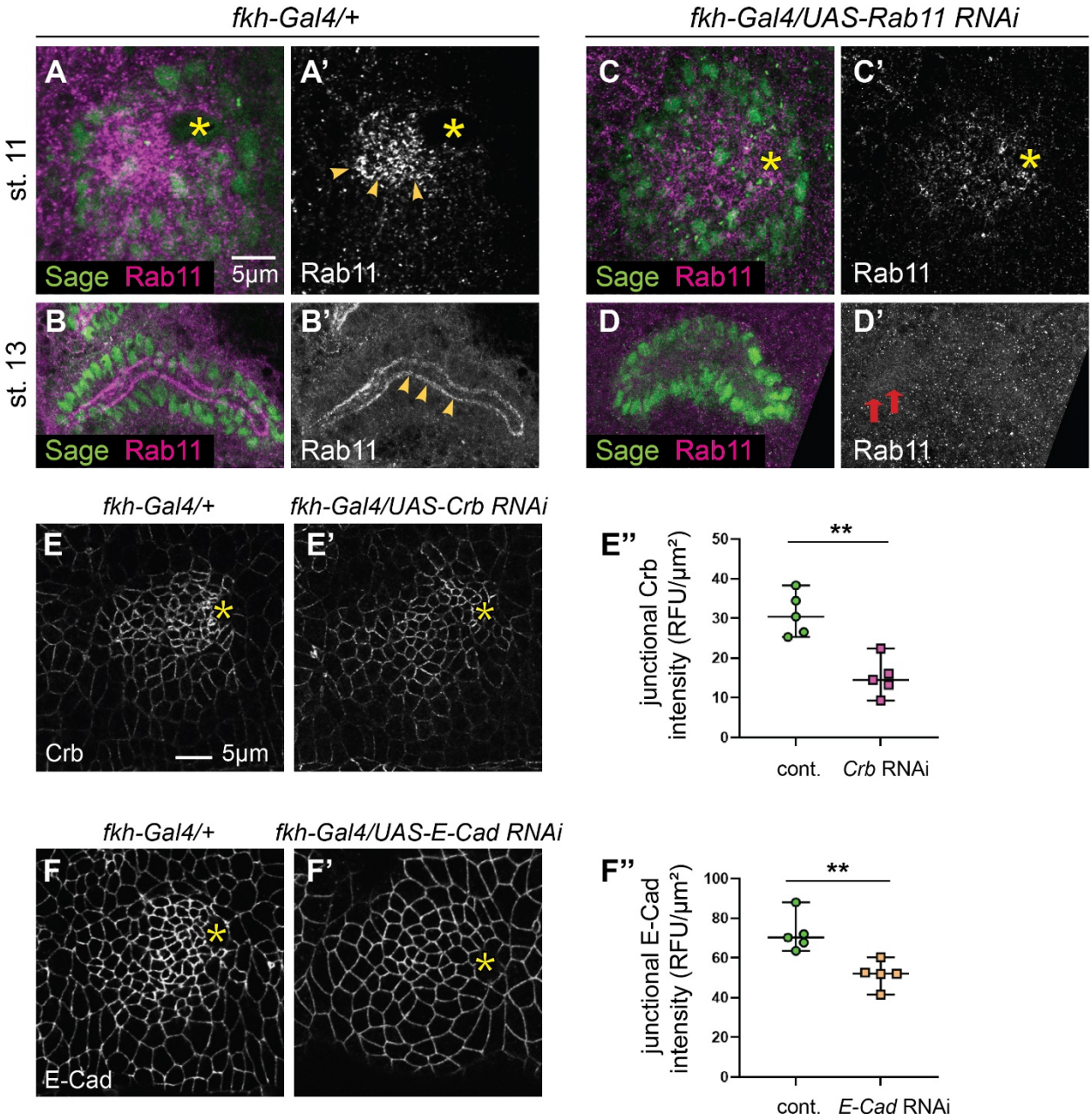

835 **Figure S4. MTs play a role in apical localization of Rab11 and apical transport of**
836 **Crb and E-Cad throughout SG formation.** (A-B’’’) Confocal images of stage 16 control
837 (A-A’’’) and spastin-overexpressing (B-B’’’) SGs immunostained for Rab11 and Nuf. In
838 control, Rab11 and Nuf localize in the apical region of SG cells (red arrowheads in A’’ and
839 A’’’). In spastin-overexpressing SGs, Rab11 and Nuf are mislocalized to aggregates in
840 the cytoplasm of cells (yellow arrowheads in B’-B’’’). (C-E’’) Confocal images of stage 13
841 control (C-C’’), spastin-overexpressing (D-D’’) and *Rab11* RNAi (E-E’’) SGs
842 immunostained for Sage (SG nuclei), E-Cad and Fog. (C’-E’) Compared to strong E-Cad
843 signals primarily at adherens junctions in the control SG (C’), strong lateral E-Cad signals
844 are shown in spastin-overexpressing and *Rab11* RNAi SG (blue arrows in E’). Insets,
845 higher magnification of the yellow boxed regions in C’-E’. (C’’-E’’) Compared to strong
846 apical Fog signals in the control SG (C’’), Fog signals are very weak in spastin-
847 overexpressing (D’’) and *Rab11* RNAi (E’’) SGs. (F-G’’’) Confocal images of stage 16 SGs
848 stained for Crb and Rab11. (F-F’’’) Overexpression of Crb causes mislocalization of Crb
849 (green) to all membrane domains and expands membranes. Rab11 is still enriched in the
850 apical domain (red arrowheads). (G-G’’’) Co-overexpression of spastin and Crb results in
851 mislocalization of Crb to large aggregates in the cytoplasm, which overlap with Rab11
852 (yellow arrowheads). (H-I’’’) Confocal images of stage 16 SGs immunostained for E-Cad
853 and Rab11. (H-H’’’) In the control SG, the majority of E-Cad signals are detected at
854 adherens junctions (red arrowheads). Small punctate E-Cad signals are occasionally
855 shown in the basolateral region (blue arrows). (I-I’’’) Co-overexpression of E-Cad and
856 spastin causes mislocalization of E-Cad to cytoplasmic aggregates, which overlap with
857 Nuf (yellow arrowheads). White dashed line, cell and nuclear boundaries (A’, B’) and
858 apical membrane (F’, H’, I’). Nu, nucleus.

859

Supplemental Figure 4

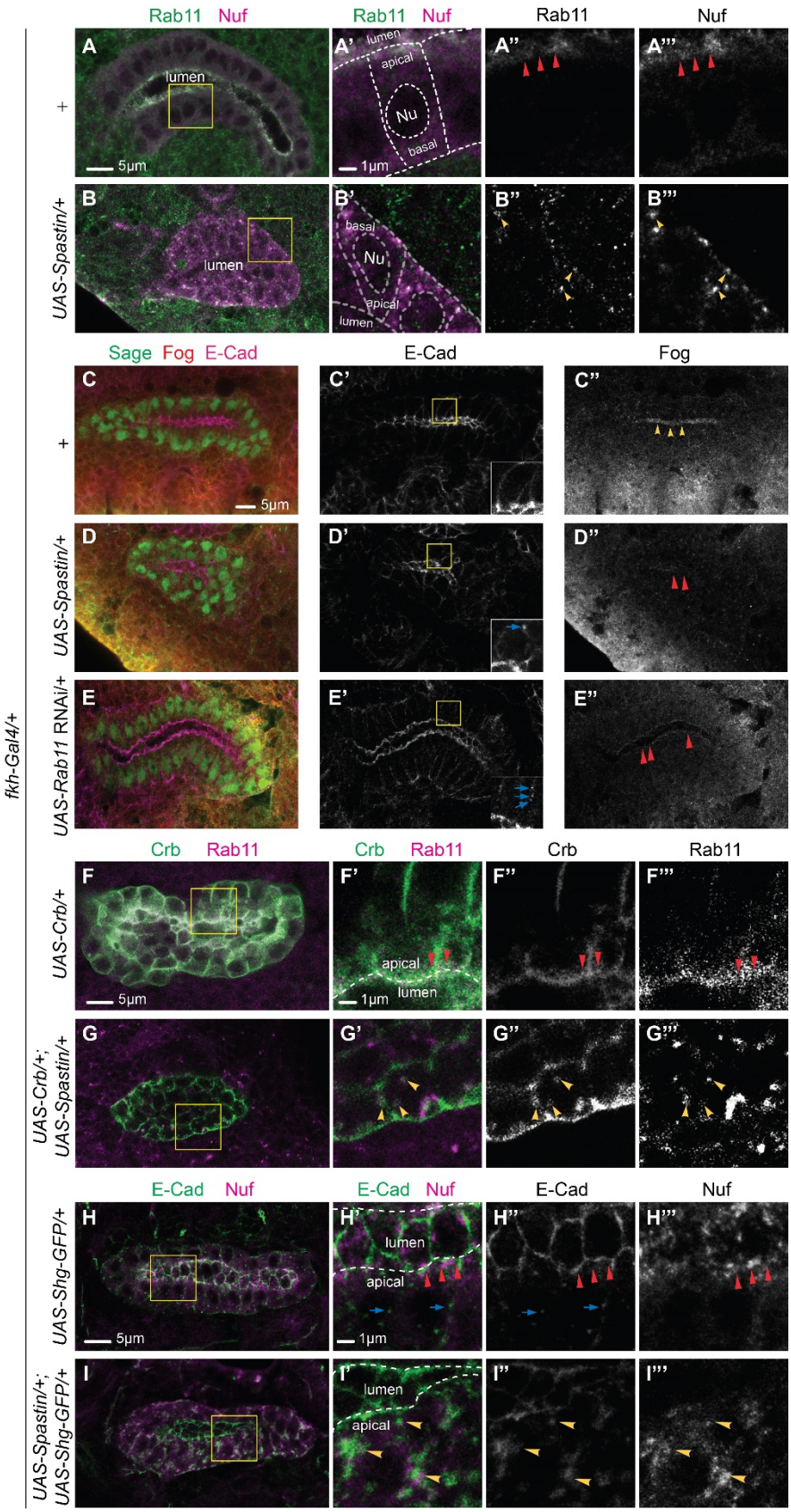

860

861 **Fly genotypes**

Figures	**Genotypes**
Figure 1B-F''''	*Oregon R*
Figure 2A-B'', E-E'	*Oregon R*
Figure 2C-C'''	*fkh-Gal4/+*
Figure 2D-D''', F-F'	*fkh-Gal4/UAS-Spastin-CFP*
Figure 3A-A'	*fkh-Gal4/+*
Figure 3B-B'	*fkh-Gal4/UAS-Rab11-S25N-YFP*
Figure 3C-C'	*fkh-Gal4/UAS-Rab11* RNAi (TRiP.JF02812)
Figure 3D-D'	*UAS-Dicer-2/+; fkh-Gal4/UAS-Dhc64C* RNAi (GD12258)
Figure 3E-E'	*Oregon R*
Figure 3F-F'	*klar*^{1}
Figure 3I-I''	*UAS-Dicer-2/+; fkh-Gal4/+*
Figure 3J-J''	*UAS-Dicer-2/+; fkh-Gal4/UAS-Dhc64C RNAi* (GD12258)
Figure 3K-K''	*Oregon R*
Figure 3L-L''	*klar*^{mCD4}
Figure 4A-A''''	*sqh-GFP/+; fkh-Gal4/+*
Figure 4B-B''''	*sqh-GFP/UAS-Dicer-2; fkh-Gal4/UAS-Rab11* RNAi (UAS-Rab11.dsRNA.WIZ)
Figure 4F-F''	*fkh-Gal4 ubi-Rok-GFP/+*

Figure 4G-G''	*UAS-Dicer-2/+; fkh-Gal4 ubi-Rok-GFP/UAS-Rab11* RNAi (UAS-Rab11.dsRNA.WIZ)
Figure 5A-A'	*sqh-GFP/+; fkhGal4/+*
Figure 5B-B'	*sqh-GFP/UAS-Dicer-2; fkh-Gal4/UAS-Dhc64C* RNAi (GD12258)
Figure 5F-F'	*sqh-GFP; sqh^{AX3}*
Figure 5G-G'	*sqh-GFP; klar^{1}*
Figure 5K-K'	*fkh-Gal4 ubi-Rok-GFP/+*
Figure 5L-L'	*UAS-Spastin/+; fkh-Gal4 ubi-Rok-GFP/+*
Figure 5M-M'	*UAS-Dicer-2/+; fkh-Gal4 ubi-Rok-GFP/UAS-Dhc64C* RNAi (GD12258)
Figure 5N-N'	*ubi-Rok-GFP*
Figure 5O-O'	*klar^{mCD4} ubi-Rok-GFP*
Figure 6A-A''', D-D''''	*fkh-Gal4/+*
Figure 6B-B''', E-E''''	*fkh-Gal4/UAS-Spastin*
Figure 6C-C''', F-F''''	*fkh-Gal4/UAS-Rab11* RNAi (TRiP.JF02812)
Figure 7A-A'	*fkh-Gal4/+*
Figure 7B-B''	*fkh-Gal4/UAS-Crb RNAi* (TRiP. HMS01409)
Figure 7C-C'	*fkh-Gal4/UAS-E-Cad* RNAi (TRiP.HMS00693)
Figure 8A-A''	*sqh-GFP/+; fkh-Gal4/+*

Figure 8B-B''	*sqh-GFP/+; fkh-Gal4/UAS-Crb* RNAi (TRiP.HMS01409)
Figure 8C-C''	*sqh-GFP/+; fkh-Gal4/UAS-E-Cad* RNAi (TRiP.HMS00693)
Figure 8D-D''	*fkh-Gal4 ubi-Rok-GFP/+*
Figure 8E-E''	*fkh-Gal4 ubi-Rok-GFP/UAS-Crb* RNAi (TRiP.HMS01409)
Figure 8F-F''	*fkh-Gal4 ubi-Rok-GFP/UAS-E-Cad* RNAi (TRiP.HMS00693)
Figure S1A-A'''''	*Rab11-EYFP*
Figure S1B-B'''	*Rab5-EYFP*
Figure S1D-D'''	*Rab7-EYFP*
Figure S1E-E'''	*Oregon R*
Figure S2A-A''	*fkh-Gal4/+*
Figure S2B-B''	*fkh-Gal4/UAS-Spastin-CFP*
Figure S3A-A', B-B', E, F	*fkh-Gal4/+*
Figure S3C-C', D-D'	*fkh-Gal4/UAS-Rab11* RNAi (TRiP.JF02812)
Figure S3E'	*fkh-Gal4/UAS-Crb* RNAi (TRiP.HMS01409)
Figure S3F'	*fkh-Gal4/UAS-E-Cad* RNAi (TRiP.HMS00693)
Figure S4A-A''', C-C''	*fkh-Gal4/+*
Figure S4B-B''', D-D''	*fkh-Gal4/UAS-Spastin*
Figure S4E-E''	*fkh-Gal4/UAS-Rab11* RNAi (TRiP.JF02812)

Figure S4F-F’’’	*UAS-Crb/+; fkh-Gal4/+*
Figure S4G-G’’’	*UAS-Crb/+; fkh-Gal4/UAS-Spastin*
Figure S4H-H’’’	*fkh-Gal4/UAS-Shg-GFP*
Figure S4I-I’’’	*UAS-Spastin/+; fkh-Gal4/UAS-Shg-GFP*

862

863

864

865 ## References

866 Abreu-Blanco, M.T., Verboon, J.M., and Parkhurst, S.M. (2014). Coordination of Rho family GTPase
867 activities to orchestrate cytoskeleton responses during cell wound repair. Curr Biol *24*, 144-155.
868 Aguilar-Aragon, M., Fletcher, G., and Thompson, B.J. (2020). The cytoskeletal motor proteins Dynein and
869 MyoV direct apical transport of Crumbs. Dev Biol *459*, 126-137.
870 Anborgh, P.H., Seachrist, J.L., Dale, L.B., and Ferguson, S.S. (2000). Receptor/beta-arrestin complex
871 formation and the differential trafficking and resensitization of beta2-adrenergic and angiotensin II type
872 1A receptors. Mol Endocrinol *14*, 2040-2053.
873 Andrew, D.J., and Ewald, A.J. (2010). Morphogenesis of epithelial tubes: Insights into tube formation,
874 elongation, and elaboration. Dev Biol *341*, 34-55.
875 Benton, M.A., Frey, N., Nunes da Fonseca, R., von Levetzow, C., Stappert, D., Hakeemi, M.S., Conrads,
876 K.H., Pechmann, M., Panfilio, K.A., Lynch, J.A.*, et al.* (2019). Fog signaling has diverse roles in epithelial
877 morphogenesis in insects. Elife *8*.
878 Booth, A.J.R., Blanchard, G.B., Adams, R.J., and Roper, K. (2014). A dynamic microtubule cytoskeleton
879 directs medial actomyosin function during tube formation. Dev Cell *29*, 562-576.
880 Burbank, K.S., Groen, A.C., Perlman, Z.E., Fisher, D.S., and Mitchison, T.J. (2006). A new method reveals
881 microtubule minus ends throughout the meiotic spindle. J Cell Biol *175*, 369-375.
882 Cerniello, F.M., Carretero, O.A., Longo Carbajosa, N.A., Cerrato, B.D., Santos, R.A., Grecco, H.E., and
883 Gironacci, M.M. (2017). MAS1 Receptor Trafficking Involves ERK1/2 Activation Through a beta-Arrestin2-
884 Dependent Pathway. Hypertension *70*, 982-989.
885 Chung, S., and Andrew, D.J. (2014). Cadherin 99C regulates apical expansion and cell rearrangement
886 during epithelial tube elongation. Development *141*, 1950-1960.
887 Chung, S., Hanlon, C.D., and Andrew, D.J. (2014). Building and specializing epithelial tubular organs: the
888 Drosophila salivary gland as a model system for revealing how epithelial organs are specified, form and
889 specialize. Wiley Interdiscip Rev Dev Biol *3*, 281-300.
890 Chung, S., Kim, S., and Andrew, D.J. (2017). Uncoupling apical constriction from tissue invagination. Elife
891 *6*.
892 Dale, L.B., Seachrist, J.L., Babwah, A.V., and Ferguson, S.S. (2004). Regulation of angiotensin II type 1A
893 receptor intracellular retention, degradation, and recycling by Rab5, Rab7, and Rab11 GTPases. J Biol
894 Chem *279*, 13110-13118.
895 David, D.J., Tishkina, A., and Harris, T.J. (2010). The PAR complex regulates pulsed actomyosin
896 contractions during amnioserosa apical constriction in Drosophila. Development *137*, 1645-1655.
897 Du, F., Ozdowski, E.F., Kotowski, I.K., Marchuk, D.A., and Sherwood, N.T. (2010). Functional conservation
898 of human Spastin in a Drosophila model of autosomal dominant-hereditary spastic paraplegia. Hum Mol
899 Genet *19*, 1883-1896.
900 Dunst, S., Kazimiers, T., von Zadow, F., Jambor, H., Sagner, A., Brankatschk, B., Mahmoud, A., Spannl, S.,
901 Tomancak, P., Eaton, S.*, et al.* (2015). Endogenously tagged rab proteins: a resource to study membrane
902 trafficking in Drosophila. Dev Cell *33*, 351-365.
903 Elting, M.W., Hueschen, C.L., Udy, D.B., and Dumont, S. (2014). Force on spindle microtubule minus ends
904 moves chromosomes. J Cell Biol *206*, 245-256.
905 Fan, G.H., Lapierre, L.A., Goldenring, J.R., and Richmond, A. (2003). Differential regulation of CXCR2
906 trafficking by Rab GTPases. Blood *101*, 2115-2124.
907 Flores-Benitez, D., and Knust, E. (2015). Crumbs is an essential regulator of cytoskeletal dynamics and
908 cell-cell adhesion during dorsal closure in Drosophila. Elife *4*.
909 Gorvel, J.P., Chavrier, P., Zerial, M., and Gruenberg, J. (1991). rab5 controls early endosome fusion in
910 vitro. Cell *64*, 915-925.

911 Goshima, G., Nedelec, F., and Vale, R.D. (2005). Mechanisms for focusing mitotic spindle poles by minus
912 end-directed motor proteins. J Cell Biol *171*, 229-240.
913 Gross, S.P., Welte, M.A., Block, S.M., and Wieschaus, E.F. (2000). Dynein-mediated cargo transport in
914 vivo. A switch controls travel distance. J Cell Biol *148*, 945-956.
915 Guglielmi, G., Barry, J.D., Huber, W., and De Renzis, S. (2015). An Optogenetic Method to Modulate Cell
916 Contractility during Tissue Morphogenesis. Dev Cell *35*, 646-660.
917 Hamelin, E., Theriault, C., Laroche, G., and Parent, J.L. (2005). The intracellular trafficking of the G
918 protein-coupled receptor TPbeta depends on a direct interaction with Rab11. J Biol Chem *280*, 36195-
919 36205.
920 Heald, R., Tournebize, R., Blank, T., Sandaltzopoulos, R., Becker, P., Hyman, A., and Karsenti, E. (1996).
921 Self-organization of microtubules into bipolar spindles around artificial chromosomes in Xenopus egg
922 extracts. Nature *382*, 420-425.
923 Hunyady, L., Baukal, A.J., Gaborik, Z., Olivares-Reyes, J.A., Bor, M., Szaszak, M., Lodge, R., Catt, K.J., and
924 Balla, T. (2002). Differential PI 3-kinase dependence of early and late phases of recycling of the
925 internalized AT1 angiotensin receptor. J Cell Biol *157*, 1211-1222.
926 Innamorati, G., Le Gouill, C., Balamotis, M., and Birnbaumer, M. (2001). The long and the short cycle.
927 Alternative intracellular routes for trafficking of G-protein-coupled receptors. J Biol Chem *276*, 13096-
928 13103.
929 Izquierdo, E., Quinkler, T., and De Renzis, S. (2018). Guided morphogenesis through optogenetic
930 activation of Rho signalling during early Drosophila embryogenesis. Nat Commun *9*, 2366.
931 Jha, A., van Zanten, T.S., Philippe, J.M., Mayor, S., and Lecuit, T. (2018). Quantitative Control of GPCR
932 Organization and Signaling by Endocytosis in Epithelial Morphogenesis. Curr Biol *28*, 1570-1584 e1576.
933 Jouette, J., Guichet, A., and Claret, S.B. (2019). Dynein-mediated transport and membrane trafficking
934 control PAR3 polarised distribution. Elife *8*.
935 Kerridge, S., Munjal, A., Philippe, J.M., Jha, A., de las Bayonas, A.G., Saurin, A.J., and Lecuit, T. (2016).
936 Modular activation of Rho1 by GPCR signalling imparts polarized myosin II activation during
937 morphogenesis. Nat Cell Biol *18*, 261-270.
938 Khanal, I., Elbediwy, A., Diaz de la Loza Mdel, C., Fletcher, G.C., and Thompson, B.J. (2016). Shot and
939 Patronin polarise microtubules to direct membrane traffic and biogenesis of microvilli in epithelia. J Cell
940 Sci *129*, 2651-2659.
941 Khodjakov, A., Copenagle, L., Gordon, M.B., Compton, D.A., and Kapoor, T.M. (2003). Minus-end capture
942 of preformed kinetochore fibers contributes to spindle morphogenesis. J Cell Biol *160*, 671-683.
943 Ko, C.S., Tserunyan, V., and Martin, A.C. (2019). Microtubules promote intercellular contractile force
944 transmission during tissue folding. J Cell Biol *218*, 2726-2742.
945 Laan, L., Pavin, N., Husson, J., Romet-Lemonne, G., van Duijn, M., Lopez, M.P., Vale, R.D., Julicher, F.,
946 Reck-Peterson, S.L., and Dogterom, M. (2012). Cortical dynein controls microtubule dynamics to
947 generate pulling forces that position microtubule asters. Cell *148*, 502-514.
948 Langevin, J., Morgan, M.J., Sibarita, J.B., Aresta, S., Murthy, M., Schwarz, T., Camonis, J., and Bellaiche, Y.
949 (2005). Drosophila exocyst components Sec5, Sec6, and Sec15 regulate DE-Cadherin trafficking from
950 recycling endosomes to the plasma membrane. Dev Cell *9*, 365-376.
951 Le Droguen, P.M., Claret, S., Guichet, A., and Brodu, V. (2015). Microtubule-dependent apical restriction
952 of recycling endosomes sustains adherens junctions during morphogenesis of the Drosophila tracheal
953 system. Development *142*, 363-374.
954 Lee, J.Y., and Harland, R.M. (2010). Endocytosis is required for efficient apical constriction during
955 Xenopus gastrulation. Curr Biol *20*, 253-258.
956 Letizia, A., Sotillos, S., Campuzano, S., and Llimargas, M. (2011). Regulated Crb accumulation controls
957 apical constriction and invagination in Drosophila tracheal cells. J Cell Sci *124*, 240-251.

958 Li, M., McGrail, M., Serr, M., and Hays, T.S. (1994). Drosophila cytoplasmic dynein, a microtubule motor
959 that is asymmetrically localized in the oocyte. J Cell Biol *126*, 1475-1494.
960 Lord, S.J., Velle, K.B., Mullins, R.D., and Fritz-Laylin, L.K. (2020). SuperPlots: Communicating
961 reproducibility and variability in cell biology. J Cell Biol *219*.
962 Manning, A.J., Peters, K.A., Peifer, M., and Rogers, S.L. (2013). Regulation of epithelial morphogenesis by
963 the G protein-coupled receptor mist and its ligand fog. Sci Signal *6*, ra98.
964 Manning, A.J., and Rogers, S.L. (2014). The Fog signaling pathway: insights into signaling in
965 morphogenesis. Dev Biol *394*, 6-14.
966 Martin, A.C., and Goldstein, B. (2014). Apical constriction: themes and variations on a cellular
967 mechanism driving morphogenesis. Development *141*, 1987-1998.
968 Martin, A.C., Kaschube, M., and Wieschaus, E.F. (2009). Pulsed contractions of an actin-myosin network
969 drive apical constriction. Nature *457*, 495-499.
970 Mason, F.M., Tworoger, M., and Martin, A.C. (2013). Apical domain polarization localizes actin-myosin
971 activity to drive ratchet-like apical constriction. Nat Cell Biol *15*, 926-936.
972 Meresse, S., Gorvel, J.P., and Chavrier, P. (1995). The rab7 GTPase resides on a vesicular compartment
973 connected to lysosomes. J Cell Sci *108 (Pt 11)*, 3349-3358.
974 Miao, H., Vanderleest, T.E., Jewett, C.E., Loerke, D., and Blankenship, J.T. (2019). Cell ratcheting through
975 the Sbf RabGEF directs force balancing and stepped apical constriction. J Cell Biol.
976 Myat, M.M., and Andrew, D.J. (2000). Organ shape in the Drosophila salivary gland is controlled by
977 regulated, sequential internalization of the primordia. Development *127*, 679-691.
978 Myat, M.M., and Andrew, D.J. (2002). Epithelial tube morphology is determined by the polarized growth
979 and delivery of apical membrane. Cell *111*, 879-891.
980 Ossipova, O., Kim, K., Lake, B.B., Itoh, K., Ioannou, A., and Sokol, S.Y. (2014). Role of Rab11 in planar cell
981 polarity and apical constriction during vertebrate neural tube closure. Nat Commun *5*, 3734.
982 Rauzi, M., Lenne, P.F., and Lecuit, T. (2010). Planar polarized actomyosin contractile flows control
983 epithelial junction remodelling. Nature *468*, 1110-1114.
984 Riggs, B., Rothwell, W., Mische, S., Hickson, G.R., Matheson, J., Hays, T.S., Gould, G.W., and Sullivan, W.
985 (2003). Actin cytoskeleton remodeling during early Drosophila furrow formation requires recycling
986 endosomal components Nuclear-fallout and Rab11. J Cell Biol *163*, 143-154.
987 Roeth, J.F., Sawyer, J.K., Wilner, D.A., and Peifer, M. (2009). Rab11 helps maintain apical crumbs and
988 adherens junctions in the Drosophila embryonic ectoderm. PLoS One *4*, e7634.
989 Rogers, S.L., Wiedemann, U., Hacker, U., Turck, C., and Vale, R.D. (2004). Drosophila RhoGEF2 associates
990 with microtubule plus ends in an EB1-dependent manner. Curr Biol *14*, 1827-1833.
991 Roper, K. (2012). Anisotropy of Crumbs and aPKC drives myosin cable assembly during tube formation.
992 Dev Cell *23*, 939-953.
993 Royou, A., Field, C., Sisson, J.C., Sullivan, W., and Karess, R. (2004). Reassessing the role and dynamics of
994 nonmuscle myosin II during furrow formation in early Drosophila embryos. Mol Biol Cell *15*, 838-850.
995 Sanchez-Corrales, Y.E., Blanchard, G.B., and Roper, K. (2018). Radially patterned cell behaviours during
996 tube budding from an epithelium. Elife *7*.
997 Sawyer, J.M., Harrell, J.R., Shemer, G., Sullivan-Brown, J., Roh-Johnson, M., and Goldstein, B. (2010).
998 Apical constriction: a cell shape change that can drive morphogenesis. Dev Biol *341*, 5-19.
999 Sherwood, N.T., Sun, Q., Xue, M., Zhang, B., and Zinn, K. (2004). Drosophila spastin regulates synaptic
1000 microtubule networks and is required for normal motor function. PLoS Biol *2*, e429.
1001 Sidor, C., Stevens, T.J., Jin, L., Boulanger, J., and Roper, K. (2020). Rho-Kinase Planar Polarization at
1002 Tissue Boundaries Depends on Phospho-regulation of Membrane Residence Time. Dev Cell *52*, 364-378
1003 e367.
1004 Takeda, M., Sami, M.M., and Wang, Y.C. (2018). A homeostatic apical microtubule network shortens
1005 cells for epithelial folding via a basal polarity shift. Nat Cell Biol *20*, 36-45.

1006 Tan, R., Foster, P.J., Needleman, D.J., and McKenney, R.J. (2018). Cooperative Accumulation of Dynein-
1007 Dynactin at Microtubule Minus-Ends Drives Microtubule Network Reorganization. Dev Cell *44*, 233-247
1008 e234.
1009 Ullrich, O., Reinsch, S., Urbe, S., Zerial, M., and Parton, R.G. (1996). Rab11 regulates recycling through
1010 the pericentriolar recycling endosome. J Cell Biol *135*, 913-924.
1011 Urbansky, S., Gonzalez Avalos, P., Wosch, M., and Lemke, S. (2016). Folded gastrulation and T48 drive
1012 the evolution of coordinated mesoderm internalization in flies. Elife *5*.
1013 Volpicelli, L.A., Lah, J.J., Fang, G., Goldenring, J.R., and Levey, A.I. (2002). Rab11a and myosin Vb regulate
1014 recycling of the M4 muscarinic acetylcholine receptor. J Neurosci *22*, 9776-9784.
1015 Westermann, S., and Weber, K. (2003). Post-translational modifications regulate microtubule function.
1016 Nat Rev Mol Cell Biol *4*, 938-947.
1017 Wichmann, H., Hengst, L., and Gallwitz, D. (1992). Endocytosis in yeast: evidence for the involvement of
1018 a small GTP-binding protein (Ypt7p). Cell *71*, 1131-1142.
1019 Wodarz, A., Grawe, F., and Knust, E. (1993). CRUMBS is involved in the control of apical protein targeting
1020 during Drosophila epithelial development. Mech Dev *44*, 175-187.
1021 Yvon, A.M., Gross, D.J., and Wadsworth, P. (2001). Antagonistic forces generated by myosin II and
1022 cytoplasmic dynein regulate microtubule turnover, movement, and organization in interphase cells. Proc
1023 Natl Acad Sci U S A *98*, 8656-8661.
1024 Zhang, J., Schulze, K.L., Hiesinger, P.R., Suyama, K., Wang, S., Fish, M., Acar, M., Hoskins, R.A., Bellen,
1025 H.J., and Scott, M.P. (2007). Thirty-one flavors of Drosophila rab proteins. Genetics *176*, 1307-1322.
1026 Zhang, X.M., Ellis, S., Sriratana, A., Mitchell, C.A., and Rowe, T. (2004). Sec15 is an effector for the Rab11
1027 GTPase in mammalian cells. J Biol Chem *279*, 43027-43034.

1028